Mean structure of the North Atlantic subtropical permanent pycnocline from in-situ observations

Charlene Feucher, Guillaume Maze, Herle Mercier

Mean Structure of the North Atlantic Subtropical Permanent Pycnocline from In Situ Observations

CHARLÈNE FEUCHER AND GUILLAUME MAZE

Laboratoire d'Océanographie Physique et Spatiale, Ifremer, Plouzané, France

HERLÉ MERCIER

Laboratoire d'Océanographie Physique et Spatiale, CNRS, Plouzané, France

(Manuscript received 3 September 2015, in final form 4 April 2016)

ABSTRACT

A new objective algorithm for the characterization of the permanent pycnocline (OAC-P) in subtropical gyres is proposed. OAC-P is based on a pragmatic analysis of vertical density gradient features to identify the permanent pycnocline: OAC-P identifies the permanent pycnocline as the stratified layer found below surface mode waters. OAC-P provides the permanent pycnocline depth, unequivocally associated with a local maximum in the stratification, and top and bottom thicknesses, associated with upward and downward decreases in stratification, respectively. OAC-P uses half Gaussian curves as asymmetric nonlinear analytical models of the stratification peak. It is the first time that an algorithm is proposed to characterize objectively the permanent pycnocline for a region where handling the stronger stratification peak of the seasonal pycnocline is complex. A guideline for how to implement the OAC-P is given, with application to the North Atlantic Ocean Argo data as an example. OAC-P provides a detailed description of the mean structure of the North Atlantic subtropical permanent pycnocline. OAC-P detects a permanent pycnocline throughout the subtropical gyre north of the North Equatorial Current. The large-scale description of the permanent pycnocline depth structure as a classic bowl shape is captured however with much more detail. New regional information is provided. In particular, (i) there is only one region—the southern recirculation gyre of the Gulf Stream extension—where the permanent pycnocline is along an isopycnal surface and (ii) vertical asymmetries clearly discriminate one region from another.

1. Introduction

The vertical stratification structure of subtropical oceanic gyres is characterized by the permanent presence of a layer with a significant vertical density gradient centered between 500 and 1000 m (Sprintall and Cronin 2001). This key subtropical oceanic feature is commonly called the permanent pycnocline (the term *pycnocline* will refer to the *permanent pycnocline*).

Although well known, a clear definition for this oceanic feature is missing. To provide such a definition, let us examine the typical profile exhibiting a pycnocline in Fig. 1. Figure 1a shows a late-summer-like profile of potential density anomaly referenced to the surface (σ_0) and a smoothed Brunt–Väisälä frequency (N^2) located in the central recirculation region of the North Atlantic subtropical gyre. The profile was sampled in November by the Argo float WMO 4900481 (cycle 68) at a time when the late-summer near-surface stratification characteristic is still present but starts to erode. From the surface to the deepest part of Argo profiles (below 1200 m), we observe an alternance of key features with weak and strong stratifications. First, we observe the surface mixed layer (small $N^2 < 10^{-5}\,\mathrm{s}^{-2}$) on top of the seasonal pycnocline (large $N^2 \simeq 8\times10^{-5}\,\mathrm{s}^{-2}$) centered here around 180 m. Below, we observe the surface mode water (Hanawa and Talley 2001) centered around 400 m (small $N^2 \simeq 1\times10^{-5}\,\mathrm{s}^{-2}$) that sits on top of the pycnocline centered around 800 m (large $N^2 \simeq 2.5\times10^{-5}\,\mathrm{s}^{-2}$). Below 1200 m, we observe the weakly stratified deep water (small $N^2 \leq 0.5\times10^{-5}\,\mathrm{s}^{-2}$). Figure 1b shows the

Corresponding author address: Charlène Feucher, Laboratoire d'Océanographie Physique et Spatiale, Ifremer, CS 10070, 29280 Plouzané, France.
E-mail: charlene.feucher@ifremer.fr

DOI: 10.1175/JTECH-D-15-0192.1

Publisher's Note: This article was revised on 23 June 2016 to fix a typographical error in the corresponding author's email address that was present when originally published.

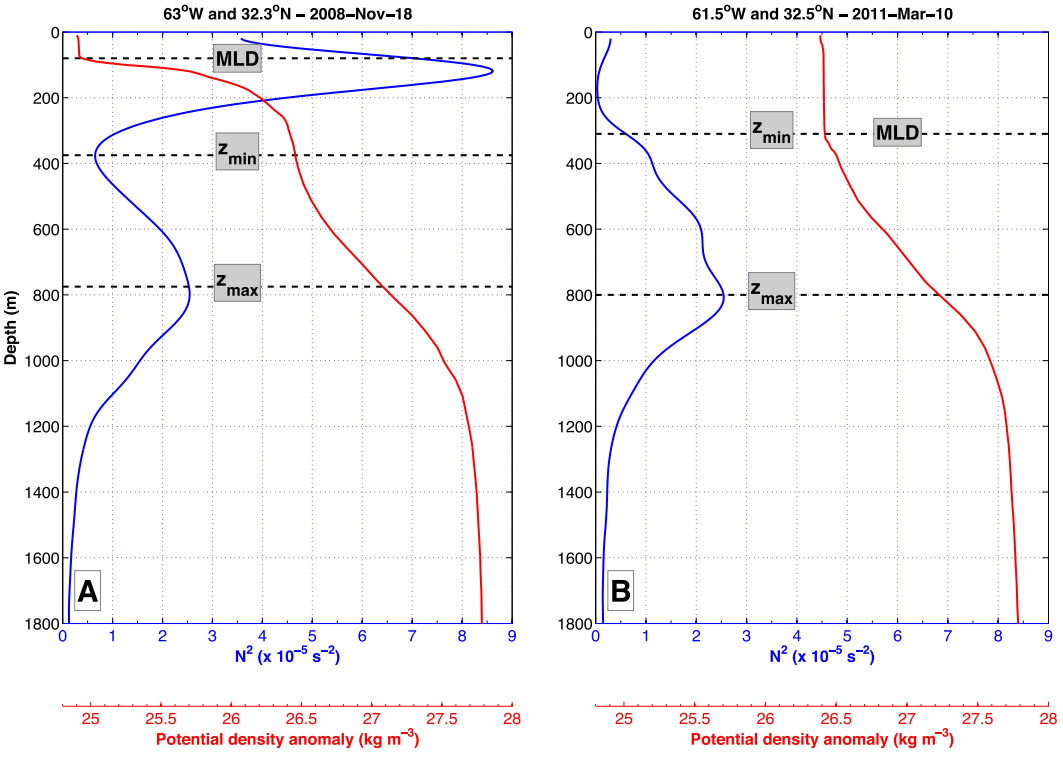

FIG. 1. Typical density profiles (red curves) in the North Atlantic subtropical gyre and N^2 profiles (blue curves) selected from the Argo dataset. (a) Surface mode water layer is trapped between the seasonal pycnocline, at the base of the mixed layer, and the pycnocline below (WMO 4900481, cycle 68). (b) Surface mode water is ventilated and merges with the mixed layer (WMO 4900480, cycle 155). Dashed horizontal black lines indicate, from top to bottom, MLD, z_{min}, and z_{max}. Profiles of N^2 are smoothed out onto scales smaller than 50 m.

same variables but as observed in late winter by the Argo float WMO 4900480 (cycle 155). The summer near-surface stratification was modified in the following way: the seasonal pycnocline vanished, and the surface mode water was ventilated and merged with the mixed layer. This profile was sampled in mid-March at a time when the surface restratification already started for a couple of days. This is why the mixed layer clearly extends down to 300 m, but the potential density anomaly is seen to decrease near the surface, explaining why N^2 increases above 200 m. From this illustration, one can simply define the pycnocline by the depth and the thickness of the stratified layer found below the surface mode water. This definition is the cornerstone of this study.

The pycnocline layer delimits important heat and anthropogenic carbon reservoirs, especially in the North Atlantic Ocean, and these reservoirs are changing under the influence of anthropogenic forcings (Pérez et al. 2013). Based on the most recent estimates for the 1975–2009 period, the rate of warming of the ocean shallower than 700 m is $0.38 \pm 0.03\,\mathrm{W\,m^{-2}}$: 3–4 times larger than in the deeper ocean below 700 m (Balmaseda et al. 2013). Similarly, for the 1955–2010 period, Levitus et al. (2012) found that the layer 700–2000 m warmed at a rate about one-third that of the upper 700-m layer. These observed trends of the heat content translate into changes in the large-scale stratification that are projected to persist in the future (IPCC et al. 2013). For instance, Capotondi et al. (2012) used 10 CMIP3 climate simulations (under SRES A2 scenario) to show that the density difference between the surface and 200 m will increase during the second half of the twenty-first century. Matear and Hirst (2003) showed that, according to a greenhouse gas forcing experiment where the level of CO_2 followed the IS92a radiative forcing scenario, the global density difference between the surface and 1700 m will double by 2100. Thus, it is essential to our understanding of these trends and of the low-frequency variability of the oceanic stratification to be able to characterize precisely key stratification features such as the pycnocline in the subtropics.

Most of the literature and characterization techniques refer to the pycnoclines of the equatorial and tropical regions. This is because in the equatorial and tropical Pacific, pycnocline variations play a key role in the El Niño–Southern Oscillation (ENSO) dynamics. Indeed, the vertical displacement and zonal tilting of the pycnocline

participate in a feedback loop with winds and air–sea fluxes, which has global meteorological impacts (Sarachik and Cane 2010). Therefore, numerous methods to characterize the pycnocline were developed in the equatorial and tropical regions (see the review in Fiedler 2010). The most popular method is the *representative isotherm*, which approximates the depth of the pycnocline by the depth of a carefully selected isotherm, often the 20°C isotherm because it is located near the center of the thermocline (Donguy 1987; Kessler 1990; Kessler et al. 1995). But this method cannot describe the thickness of the pycnocline. Other methods based on segments fitted to the density profile can provide pycnocline thickness estimates but are then limited to a linear approximation of the stratification within the pycnocline. Despite some refinements, such as a location-dependent representative isotherm (Wang et al. 2000), these methods remain adapted only to the low-latitude pycnocline. In other words, they are based on the fact that their targeted pycnocline always corresponds to the first maximum in the vertical density gradient. This makes them inappropriate to the characterization of the subtropical pycnocline associated with the second maximum in the density gradient (the first one being linked to the seasonal pycnocline; see Fig. 1).

In the oceanic heat uptake and meridional overturning circulation literature, one can also find pycnocline characterization methods. They are mostly inspired by Gnanadesikan (1999) and Gnanadesikan et al. (2007), who proposed a general method based on the depth of the barycenter of the water column, that is, the depth of the first moment of the density distribution. Consequently, one can define the pycnocline thickness using the second moment of the density distribution. Fučkar (2010) developed a semiempirical model of the pycnocline based on such methods. Although very elegant and useful for theoretical studies, these methods cannot handle the complex and seasonally varying stratification structure of the subtropics with multiple peaks. This is because all moment-based methods assume a monotonic density profile with a sigmoid shape that cannot represent a seasonal pycnocline nor a surface mode water.

In this study, we propose an algorithm to characterize the pycnocline of the subtropics, on the poleward side of the north/south equatorial currents, using a pragmatic analysis of the stratification that can take into account the overlying seasonal pycnocline and be used with both observed and modeled density profiles. We use stratification, and not a representative isopycnal, to characterize the pycnocline in order to appropriately characterize the pycnocline in the scenario of long-term changes in the oceanic density. Indeed, water mass changes and isopycnal heaving or circulation can modify the depth/thickness of the pycnocline in different, if opposite, ways (Yang and Wang 2009; Fiedler et al. 2013).

The article is organized as follows. Data sources are presented in section 2. The proposed objective algorithm for the characterization of the permanent pycnocline (OAC-P) is presented in section 3 and its implementation is explained in section 4. Then, we illustrate OAC-P with Argo data in the North Atlantic Ocean in section 5. Results are discussed and conclusions are drawn in section 6.

2. Data

In this study, we characterized the observed mean structure of the pycnocline in the North Atlantic subtropical gyre using data from the Argo observational array (Riser et al. 2016). Argo data were downloaded from the FTP server of the French Global Data Assembly Center Coriolis (Argo 2014). We selected profiles between the equator and 70°N with a quality control (QC) flag on pressure, temperature, and salinity set to 1, 2, 5, or 8, which are considered as good data [see reference Table 2 in Carval et al. (2012)]. A collection of 147 069 profiles from 1452 Argo floats in the North Atlantic was obtained. The time series starts in May 1998; since 2007, the spatial/temporal distribution is nominally one profile per 3° × 3° cell every 10 days. Argo floats typically profile down to 2000 m, and most profiles have a vertical sampling scheme with a 10-m resolution above 400- or 500-m depth and a 50-m resolution below.

To evaluate the ability for OAC-P to characterize the pycnocline from profiles with different properties, we used three additional datasets. We used data from the A03 World Ocean Circulation Experiment (WOCE) section (Schlitzer 2000). We downloaded the 1993 A03 WOCE section from online (http://cchdo.ucsd.edu/). The 1993 A03 is a North Atlantic zonal section performed along 36°N. Profiles are from the surface down to the bottom of the ocean with a 2-m resolution. We also used data from the 2010 OVIDE survey (Mercier et al. 2015). Observatoire de la Variabilité Interannuelle et Décennale en Atlantique Nord (OVIDE) is a section performed from Portugal to Greenland. Profiles are from the surface down to the bottom of the ocean with a 1-m resolution. A03 WOCE and OVIDE data will be used to evaluate the ability of OAC-P to continuously characterize the pycnocline in space in two different regions and through two different frontal regions (the Gulf Stream and the North Atlantic Current).

We used time series of ship-based hydrographic profiles from the Bermuda Atlantic Time Series Study (BATS) project. This time series, begun in 1988, is a fixed-location time series. BATS CTD data were downloaded (from http://batsftp.bios.edu/) on 16 February

2015. We used data for the period October 1988 to July 2012. Profiles typically have a 2-m vertical resolution. BATS data will be used to evaluate the ability of OAC-P to continuously characterize the pycnocline in time throughout the seasonal cycle. To complete the evaluation, we will also show OAC-P results for the Argo float 4900497. This particular float circulated on the northern flank of the Gulf Stream, then crossed it, and circulated southward in the central recirculation region of the subtropical gyre during three seasonal cycles from 2004 to 2007.

For all profiles in each dataset, temperature T, salinity S, and pressure P were used to compute a profile of potential density anomaly referenced to the surface $\sigma_0 = \rho(S, \theta, P = 0) - 1000$ (Fofonoff and Millard 1983), where θ is the potential temperature, and a profile of Brunt–Väisälä frequency squared N^2 (Jackett and Mcdougall 1995) is defined as

$$N^2(z) = -\frac{g}{\rho(z)}\frac{\partial \rho(z)}{\partial z}, \tag{1}$$

where ρ is the density. Temperature, salinity, potential density anomaly σ_0, and N^2 profiles were then interpolated onto a regular depth axis going from the surface down to 2000 m with a 5-m resolution.

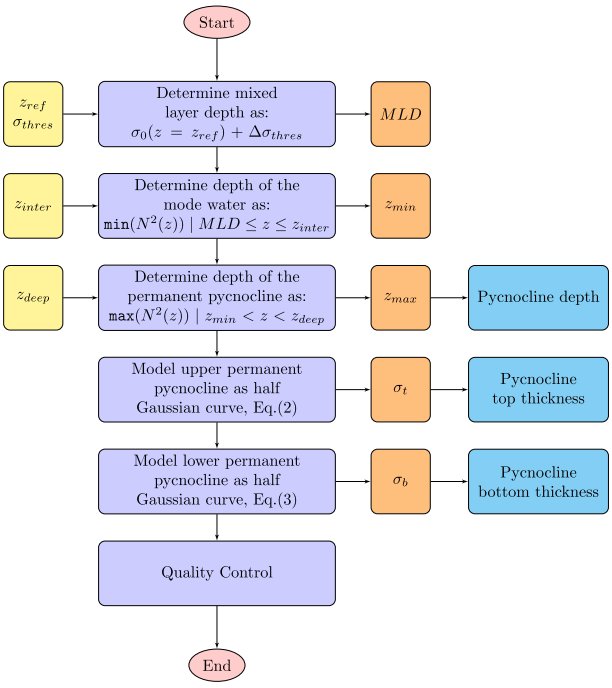

FIG. 2. Flowchart of the OAC-P algorithm to characterize the depth and thicknesses of the pycnocline. (left to right) Yellow blocks contain user-defined OAC-P input parameters, purple blocks are the main steps of the algorithm, orange blocks contain OAC-P outputs, and cyan blocks show where the depth and thicknesses of the pycnocline are computed. See section 3a for more details.

3. An algorithm to detect and characterize the pycnocline in subtropical gyres

In this section, we first describe how OAC-P processes profiles exhibiting a pycnocline (as defined in the introduction) to characterize it in terms of pycnocline depth and pycnocline thickness. Then, we illustrate and provide more details about the model we use to estimate the pycnocline thickness, a key element of OAC-P.

a. *OAC-P algorithm*

To characterize the pycnocline, one difficulty is that even though throughout the subtropical gyre the typical profile pattern (cf. Fig. 1) does not change qualitatively, stratification amplitudes, surface mode water characteristics, and pycnocline depths and thicknesses vary quantitatively. Another difficulty is that the surface mode water and the pycnocline are not an absolute minimum nor maximum in stratification (an overall maximum or minimum in N^2 cannot be used to localize them in a profile); hence, the notion of local maximum and minimum is critical.

To explain how OAC-P can objectively identify and characterize these local features, we represented in Fig. 2 the flowchart of the OAC-P algorithm. The procedure has six steps, represented by purple blocks. On the left side, yellow blocks represent parameters taken as input and, on the right side, orange blocks represent the outputs produced at the end of each step. We now describe sequentially these six steps.

1) Step 1: First, the mixed layer depth (MLD) is computed from the potential density anomaly profile using a classic density threshold σ_{thres} from a near-surface reference depth z_{ref} (De Boyer Montégut et al. 2004).
2) Step 2: Next, to identify the depth of the surface mode water, the layer below the mixed layer is considered by OAC-P. The depth of the surface mode water is not simply the depth of the absolute N^2 minimum below the mixed layer. Indeed, the deep waters have smaller stratification value (typically $N^2 \simeq 10^{-5}\,\text{s}^{-2}$) than the surface mode waters (typically $N^2 \simeq 10^{-6}\,\text{s}^{-2}$). To face this challenge, OAC-P users must define the deepest expected values of the surface mode water depth—say, z_{inter}—and OAC-P computes the depth of the surface mode water as the depth of the N^2 minimum between MLD and z_{inter}, namely, z_{min}. The seasonality of the surface mode water is taken into account by OAC-P, which

automatically sets the depth of the surface mode water at the depth of the mixed layer when they merge (such as illustrated in Fig. 1b).

3) Step 3: Subsequently, the pycnocline can be characterized considering the depth range z_{min} to z_{deep}. Users set z_{deep} as a typical level below which density profiles reach the less stratified deep-water properties. Then OAC-P computes the depth of the pycnocline as the depth of the N^2 maximum between z_{min} and z_{deep}, namely, z_{max}. The characterization of the pycnocline depth is unequivocal; that is, there is no ambiguity in its determination once the users have defined z_{inter} and z_{deep} (two parameters discussed in detail in the next section).
4) Steps 4 and 5: The thickness of the pycnocline is characterized. More precisely, OAC-P computes two thicknesses: one for the layer above the pycnocline depth and one for the layer below the pycnocline depth. Our choice has been to model N^2 profiles with two half Gaussian curves centered on the pycnocline depth, and to define the top and bottom thicknesses of the pycnocline as their standard deviations. The total pycnocline thickness is the sum of the two layer thicknesses. These Gaussian curves $\mathscr{G}$ are defined as

$$\mathscr{G}_t(z) = B_t + A_t e^{-(z-z_{max})^2/2\sigma_t^2} \quad \text{for} \quad z_{min} \le z \le z_{max} \quad \text{and} \tag{2}$$

$$\mathscr{G}_b(z) = B_b + A_b e^{-(z-z_{max})^2/2\sigma_b^2} \quad \text{for} \quad z_{max} \le z \le z_{deep}, \tag{3}$$

where subscripts t and b stand for the top and bottom layers of the pycnocline, respectively; z is the vertical axis (positive downward); $A_{t,b} = N^2(z_{max}) - B_{t,b}$ are the relative amplitudes of the Gaussian curves; and $B_{t,b}$ are their baselines (i.e., their absolute amplitudes at infinite depth). Terms $\sigma_{t,b}$ denote the standard deviations of the Gaussian curves (their sum is the total thickness of the pycnocline). In practice and for both Gaussian curves, $B_{t,b}$ and $\sigma_{t,b}$ are optimized to obtain the best fit to the observed N^2 profile. The other parameters z_{max} and $A_{t,b}$ are computed by OAC-P from the observed N^2 profile. The amplitude A is relative—that is, not equal to $N^2(z_{max})$—because the baseline is not set to zero (i.e., the stratification is not null within the surface mode water and deep waters). Note that because there is possibly a dramatic increase in the stratification from z_{min} to the seasonal pycnocline (see Fig. 1), it is crucial to fit the top Gaussian curve to the N^2 profile below z_{min}.

The best parameters $B_{t,b}$ and $\sigma_{t,b}$ are determined separately for the top and bottom Gaussian curves as those minimizing the mean-squared error:

$$\left\| N^2(z) - \mathscr{G}_t(z \mid B_t, \sigma_t) \right\|^2 \quad \text{for} \quad z_{min} \le z \le z_{max}, \tag{4}$$

$$\left\| N^2(z) - \mathscr{G}_b(z \mid B_b, \sigma_b) \right\|^2 \quad \text{for} \quad z_{max} \le z \le z_{deep}, \tag{5}$$

using the following parameter space: $0 \le B_{t,b} \le N^2(z_{max})$ for both Gaussians and $0 \le \sigma_t \le z_{max} - z_{min}$ for the upper Gaussian and $0 \le \sigma_b \le z_{deep} - z_{max}$ for the lower Gaussian.

5) Step 6: This is where automatic and manual quality control checks on the numerical values produced by OAC-P in the previous steps are performed. These procedures are described in section 4.

b. The thickness model

Before moving on to the details of how OAC-P can be implemented following the flowchart procedure described above, it is important to illustrate and motivate our choice for the pycnocline thickness model. We illustrate in Fig. 3 that Gaussian curves are indeed appropriate to model N^2 variations around the depth of the pycnocline. Figure 3a shows a N^2 profile (in plain blue, density is in red) sampled at 27.7°N, 49.7°W (WMO 4900788, cycle 68), with a seasonal pycnocline, a surface mode water, and a pycnocline. Superimposed in dashed purple, are two best-fitted half Gaussian curves centered around the pycnocline depth at 660 m (determined following the aforementioned principles). The very good fit is obvious (between 1500 and 315 m, the RMSE is $2.22 \times 10^{-7}\,s^{-2}$). We examined more quantitatively the RMSE between the thickness model and the observed profile over the North Atlantic with the Argo dataset (not shown). We found that (i) the Gaussian model performs very well in most of the subtropical gyre and reasonably in the expected frontal region of the Gulf Stream extension (GSE) and (ii) the Gaussian model performs better than others, such as a Lorentz curve.

Figure 3b shows N^2 values and the two half Gaussian curves but plotted as a distance to the pycnocline depth. This representation highlights an asymmetric structure of the N^2 profile around the depth of the pycnocline, which was not obvious from the classic profile representation (see Fig. 3a). For this profile, going away from the depth of the pycnocline, the stratification in the upper layer decreases more rapidly than in the lower layer. More generally, our careful examination of North Atlantic subtropical N^2 profiles revealed that the peak of the stratification is not systematically found in the middle of what visually can be delimited as the transition layer between the surface mode water and deep waters. In other words, we found that the pycnocline is not systematically symmetric around its depth and we choose to use two half Gaussians in place of a single

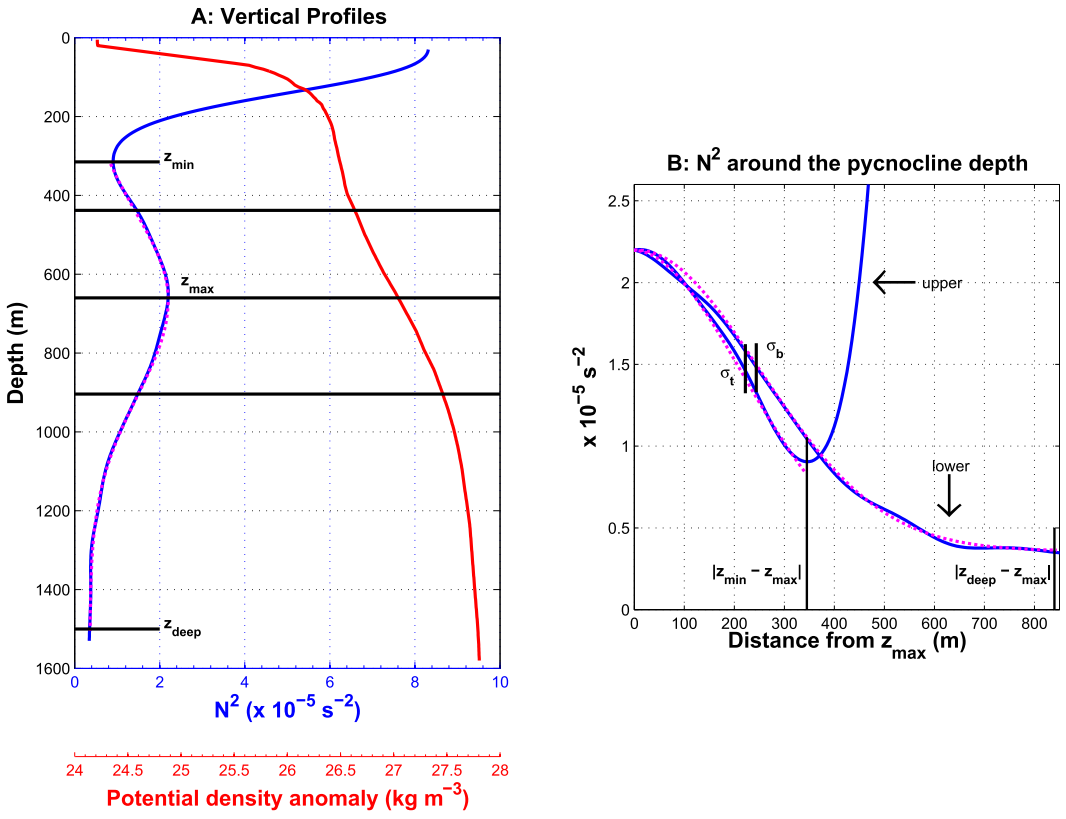

FIG. 3. Details of a vertical profile with an asymmetric pycnocline selected from the Argo dataset (WMO 4900788, cycle 68). (a) Vertical profiles of σ_0 (red) and N^2 (blue), overlaid with the two Gaussian best fits for the upper and lower portions of the N^2 profile (purple dashed). The three horizontal plain lines indicate the depth and the upper and lower limits (pycnocline depth plus/minus top/bottom thickness) of the pycnocline, as estimated from OAC-P. (b) Profiles of N^2 (blue) and the two Gaussian best fits but plotted as a distance to the pycnocline depth for the upper and lower portions of the N^2 profile (purple dashed). See section 3a for details on $\sigma_{t,b}$. Profile of N^2 has been cut at the base of the mixed layer and smoothed out onto scales smaller than 50 m.

Gaussian to model it appropriately. This will be further discussed in the application to the North Atlantic Ocean (see Fig. 9). Beyond the empirical agreement between our model and observed profiles, more physically meaningful arguments for the model applicability will be discussed in the last section of this paper.

4. OAC-P implementation

In this section, we present how to implement OAC-P with specific application to in situ data in the North Atlantic Ocean. This should be considered as an example of how to implement OAC-P. With another dataset or region, one will have to adapt the OAC-P parameters.

a. OAC-P's parameters

In the implementation of OAC-P, the user has to define the value of the following parameters: (i) a reference depth z_{ref} and a density threshold σ_{thres} to determine the mixed layer depth; (ii) the maximum expected depth of the surface mode water z_{inter}; and (iii) a lower boundary for the thickness model, that is, the depth where properties of deep waters are reached, z_{deep}.

MLD is computed by OAC-P using a classic density threshold method: MLD is the depth for which density has changed by a given threshold σ_{thres} with regard to the density at z_{ref}. For the North Atlantic we used a density threshold of 0.03 kg m^{-3} and a reference depth of −10 m (De Boyer Montégut et al. 2004); it is a standard choice for the determination of the MLD that provides sufficient accuracy for our study. It may happen that the first valid level of a profile is deeper than the 10-m reference depth. In this case OAC-P sets the reference depth to the first valid level if it is above 20 m; otherwise, the profile is discarded.

The deepest expected value of z_{inter} depends on the subtropical gyre studied. The main surface mode waters found in the North Atlantic basin are the subtropical mode water (STMW) in the west, also known as 18° Water (EDW; Worthington 1959), and the Subpolar

Mode Water (SPMW) in the east and in the Iceland Basin. Based on the most recent descriptions of these mode waters by Forget et al. (2011) and Brambilla and Talley (2008), we found $z_{inter} = 600$ m to be the most appropriate value for the North Atlantic subtropical gyre. Term z_{min} is updated automatically by OAC-P in the case where the surface mode water is unexpectedly found deeper than z_{inter} (see details in section 4c).

The depth where properties of less stratified deep waters are reached z_{deep} can be set for the North Atlantic to 1500 m (Talley 1996). This is basically the depth where the Upper North Atlantic Deep Water (UNADW) is found. This deep water is a mixture of Labrador Sea Water (LSW), Antarctic Intermediate Water (AAIW), and Mediterranean Water (MW) (Talley et al. 2011). More generally, z_{deep} refers to the depth where water masses formed in the high latitudes of subpolar gyres will be observed at midlatitudes.

b. Dealing with noise

We now describe how we handled the noise in measurements. Here we used observation datasets with a vertical resolution ranging from 1 m (shipboard CTDs) to 10 m/50 m (typical Argo). As the vertical resolution increases, the observed spectrum gains energy at small scales. Density variations at small scales are mostly due to internal wave trains and breaking but not all are due to physical processes; some variations may arise from measurement error or instrumental noise in some high-resolution datasets. These processes create finescale anomalies with a typical vertical scale of 1–100 m (McPhaden 1985; Li and Wang 2013). These small-scale features will inevitably add noise to OAC-P outputs if they are not filtered out. To suppress this noise, OAC-P low-pass filters N^2 profiles with a classic Gaussian filter (Weaver and Courtier 2001). Users have to define a cutoff length scale for this filter and this can be done through trial and error.

It is important to note that if the smoothing is too strong, the ability of OAC-P to detect the depth of the surface mode water is reduced, because the associated N^2 minimum could be smoothed out. Note also that N^2 peaks associated with the surface mode water and the pycnocline have different vertical length scales. The choice of the smoothing scale is thus a compromise between the necessary noise reduction (smoothing out small-scale features) and a correct detection of the surface mode water (maintaining the N^2 minimum layer structure). For observed North Atlantic profiles, from Argo and shipboard CTDs, we found that a reasonable compromise is reached for a smoothing length scale of 50 m.

Although satisfactory in most cases, it may happen that the smoothing length scale is not large enough to remove small-scale density variations and hence noise in the determination of the pycnocline depth. Indeed, for some profiles, we could observe two or more secondary peaks in the vicinity of the N^2 maximum (not shown). This issue must be fixed without increasing the smoothing scale. To do so, OAC-P systematically updates its first estimate of the pycnocline depth with the average depth of vertical levels, where N^2 is locally larger than 90% of its first estimate value. This simple method limits noise in the pycnocline depth estimate while at the same time, does not alter the initial result if the profile is not noisy.

c. Detection of the surface mode water

A key point in the characterization of the pycnocline is to correctly detect the presence of a surface mode water. To do so, OAC-P automatically determines that the N^2 minimum is significant and that user-defined parameters did not bias the results.

To ensure that OAC-P identified a significant N^2 minimum at z_{min}, and thus the depth of a surface mode water, OAC-P checks if there is a level below z_{min} where N^2 is at least 120% of $N^2(z_{min})$. The profile is discarded if this level is not found. The threshold value of 120% was determined using trial and error. Discarded profiles do not show an intermediate depth maximum in the stratification that would correspond to a pycnocline.

Term z_{min} is determined by OAC-P using the user-defined parameter z_{inter} (setting the expected surface mode water maximum depth). For the North Atlantic we set z_{inter} to 600 m (see section 4a). But the choice of z_{inter} is not appropriate for two types of profiles schematically represented in Figs. 4a and 4b: (i) profiles for which the surface mode water N^2 minimum is below z_{inter} and (ii) profiles experiencing a strong convective or mixing event and having a mixed layer deeper than z_{inter}. To address the first situation, OAC-P performs a test to ensure there would be no level between z_{inter} and z_{max} with N^2 smaller than $N^2(z_{min})$. If this scenario is encountered, then z_{min} is automatically updated by OAC-P to this level (see Fig. 4a, the first and update values of z_{min}). To address the second situation, OAC-P compares z_{inter} with MLD and if it is found shallower, then OAC-P updates z_{min} to MLD (see Fig. 4b).

d. Quality control

A QC is performed in the OAC-P estimation procedure to ensure a good characterization of the pycnocline layer (step 6 in the flowchart in Fig. 2). The overall QC procedure aims to verify that estimated pycnocline properties are within the scope of the OAC-P targeted subtropical profiles. This QC consists of automatically setting flags on profiles for which estimated pycnocline properties are suspicious.

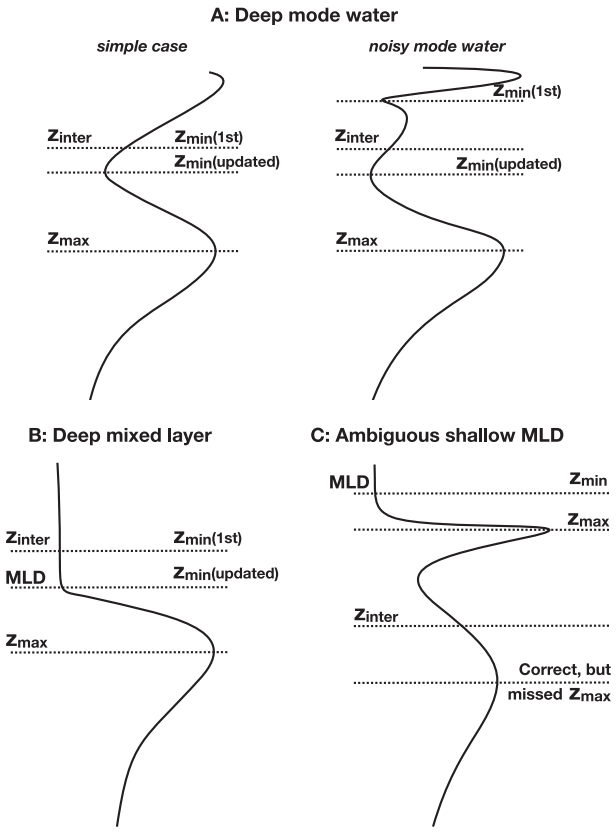

FIG. 4. Schematics of N^2 profiles misleading OAC-P estimation. (a) OAC-P parameter z_{inter} is not appropriate because the true surface mode water core is deeper: (left) the classic case and (right) the situation where a noisy signal would exhibits a minimum strictly above z_{inter}. For these profiles, OAC-P automatically updates $z_{\min}$ to the minimum between $z_{\max}$ and the first guess of $z_{\min}$. (b) OAC-P parameter z_{inter} is not appropriate because of a strong convective event creating a deeper MLD than z_{inter}. For these profiles, OAC-P automatically updates $z_{\min}$ to MLD. (c) Situation where a too shallow MLD estimate (exaggerated to illustrate the scenario) leads OAC-P to identify the seasonal pycnocline ($z_{\max}$) as the pycnocline. These profiles are detected using unambiguous neighboring good QC profiles.

A series of automatic tests performed at the end of the algorithm aim to verify that estimated parameters were not obtained using extreme values during the optimization of the thickness model. First, OAC-P assigns a specific QC flag to profiles for which the optimized $B_{t,b}$ and $\sigma_{t,b}$ parameters fall out of the 5%–95% range of the explored parameter space (see section 3a). Since those are relative values, it is thus also necessary to test absolute values. OAC-P also assigns a specific flag to profiles with a top or bottom thickness smaller than 25 m. Visual inspections of these profiles allow the user to determine whether the extreme values are indeed appropriate or whether they were reached because the range of the tested parameters was not large enough. Last, we found it useful for OAC-P to also test whether the difference at the depth of the surface mode water between N^2 given by the upper layer Gaussian model and the observed N^2 value is not too large compared to the difference between N^2 at the depth of the surface mode water and N^2 at the depth of the pycnocline. OAC-P assigns a specific QC flag if the difference is larger than 30%, that is, $[N^2(z_{\min}) - \mathcal{G}_t(z_{\min})]/[N^2(z_{\min}) - N^2(z_{\max})] > 0.3$. This test ensures that the thickness model produces an analytical profile with an end point at the mode water depth $z_{\min}$ close enough to the real profile.

When σ_{thres} is too small or when the mixed layer is affected by lateral intrusions, it may happen that the MLD estimate is too shallow and that OAC-P estimates the seasonal pycnocline instead of the pycnocline. Such ambiguous profiles are schematically represented in Fig. 4c, where we see how an MLD estimate that is too shallow leads OAC-P to identify the surface mode water within the mixed layer and hence $z_{\max}$ at the seasonal pycnocline depth. To disentangle this ambiguity, OAC-P automatically flags profiles for which $z_{\min}$ was found at the depth of the mixed layer (it concerns both the deep MLD case in Fig. 4b and the ambiguous shallow MLD in Fig. 4c). Then, OAC-P compares the depth $z_{\max}$ at which the maximum of stratification is found with that found on neighboring profiles when the surface mode water is trapped between the mixed layer and the pycnocline. In other words, OAC-P validates profiles with a wintertime structure (Fig. 1b) using neighboring unambiguous profiles with a summertime structure (Fig. 1a). For each ambiguous profile, the Gaussian distance-weighted mean and the standard deviation of neighboring good profiles are computed. The ambiguous profile is validated by OAC-P if its pycnocline depth falls within a three standard deviation range around the weighted mean of correct values; otherwise, it is discarded. This ultimate test in the OAC-P procedure ensures that it is the (permanent) pycnocline that has been characterized and not the seasonal one.

e. Evaluation

It is difficult to compare OAC-P estimates with other methods because the latter are limited and do not take into account the overlying seasonal pycnocline (see introduction). We attempted to compare OAC-P estimates with results from Gnanadesikan (1999) and Gnanadesikan et al. (2007) by using their formula for the depth and thickness of the pycnocline. However, it is difficult to make a meaningful comparison because the computational methods for the depth and thickness of the pycnocline are fundamentally different (see appendix C for more details). We therefore evaluated that OAC-P

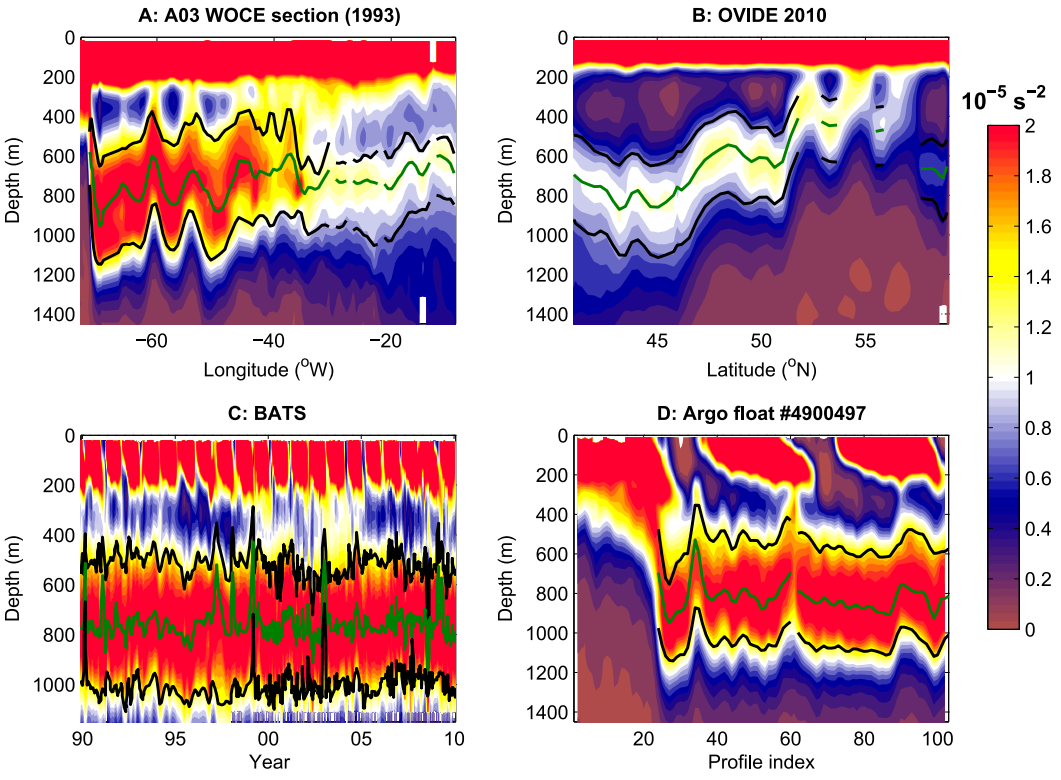

FIG. 5. OAC-P estimates on multiple datasets: color shading is the N^2 field, green line is the pycnocline depth, and the black lines are its upper and lower limits (pycnocline depth plus/minus top/bottom thickness). (a) The 1993 A03 WOCE 36°N zonal section and (b) the 2010 OVIDE section. (c) The BATS station data from 2010 to 2013 and (d) is along the trajectory of an Argo float (WMO 4900497). In (d), profile indexes from 0 to 20 correspond to the crossing of the Gulf Stream. The N^2 fields have been smoothed along the vertical to remove scales less than 50 m and along the horizontal axis to remove scales less than one station index; N^2 fields have been cut at the base of the mixed layer.

can coherently characterize the pycnocline under different conditions by using the various in situ datasets presented in section 2. The same vertical smoothing scale (50 m) was applied to all datasets.

Figure 5 shows OAC-P estimates for all datasets: the zonal A03 section at 36°N (Fig. 5a), the 10°–40°W Portugal–Greenland OVIDE section in the eastern North Atlantic (Fig. 5b), the BATS local time series (Fig. 5c), and one Argo float (WMO 4900497) crossing the Gulf Stream (Fig. 5d). For all datasets, we observe that the depth of the pycnocline is correctly estimated at middepth, where N^2 is maximum (with N^2 values around $1.8 \times 10^{-5}\,s^{-2}$ in the western part of the gyre and $1.2 \times 10^{-5}\,s^{-2}$ in the eastern part); for these regions we also observe the expected stratification minimum of surface mode waters. The estimated pycnocline thickness extends appropriately throughout the stratified layer ($N^2 > 1.4 \times 10^{-5}\,s^{-2}$ in the west, $N^2 > 1 \times 10^{-5}\,s^{-2}$ in the east), whatever the local N^2 amplitude at the depth of the pycnocline. At around 30° and 21°W in the WOCE section (Fig. 5a), OAC-P misses the pycnocline because the N^2 amplitude at the surface mode water depth is not significantly different from its amplitude at the depth of the pycnocline. Around 12°W, no pycnocline was identified because the first valid levels were deeper than 20 m. Along the OVIDE section (Fig. 5b), there is, again as expected, no pycnocline north of the subpolar front around 54°N. However, there is one valid estimate around 59°N due to a couple of profiles having the same qualitative structure as typical subtropical profiles. At the BATS station (Fig. 5c), the pycnocline is successfully characterized continuously over time and multiple seasonal cycles.

Last, along the Argo float trajectory (Fig. 5d), the pycnocline layer is coherently characterized along seasonal cycles and through the Gulf Stream. Indeed, north of the Gulf Stream (profile index from 1 to 20), no pycnocline is identified, as expected, because no surface mode water is found there. South of the Gulf Stream, the pycnocline is continuously characterized. Note that at the profile index 61, the depth of the surface mode water was not identified and the pycnocline was missed.

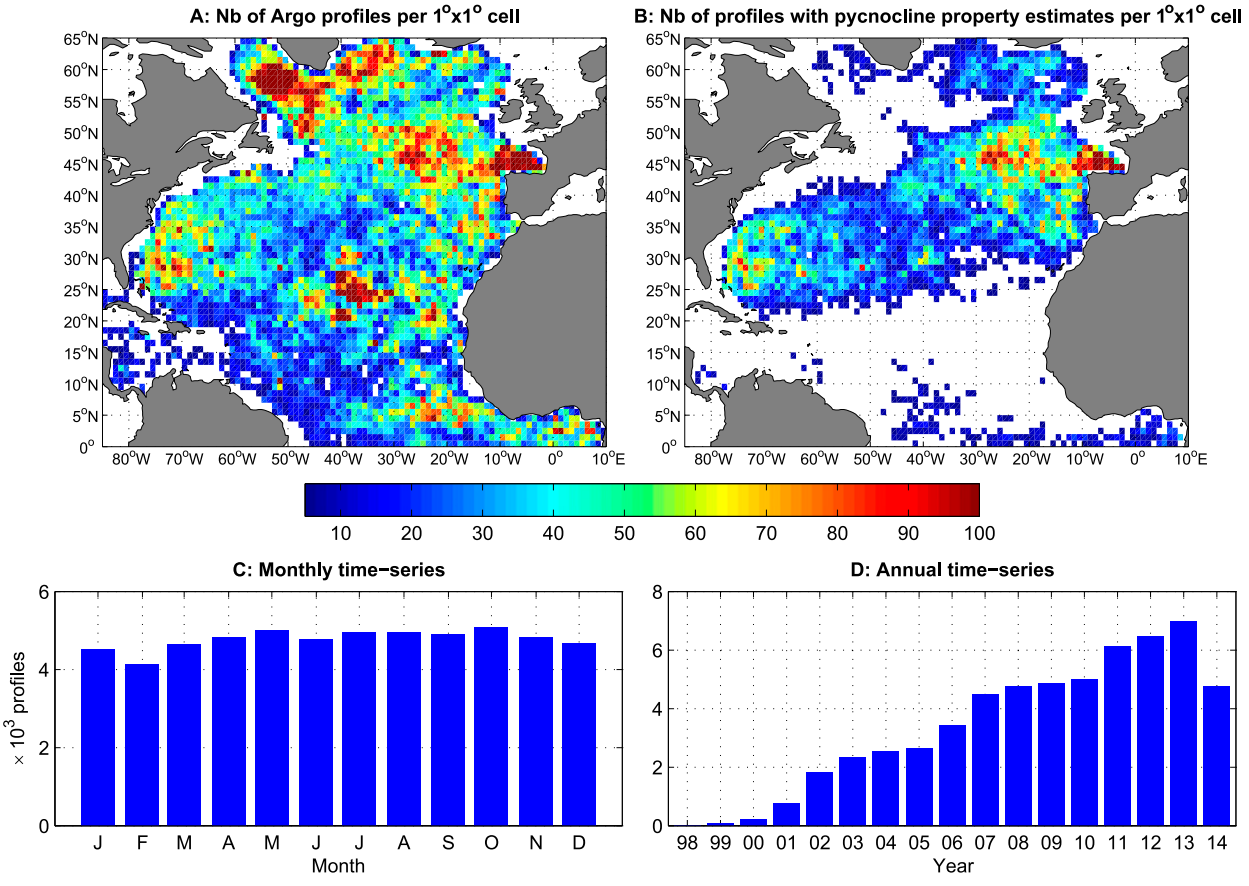

FIG. 6. (a) Number of profiles per 1° × 1° cell of the collection of 147 069 profiles in the Argo dataset used in this study. (b) Number of profiles per 1° × 1° cell of the collection of 57 297 profiles with pycnocline property estimates. White cells in (a),(b) contain fewer than five profiles. (c),(d) Seasonal and interannual sampling (number of pycnocline property estimates per month and year), respectively.

From this evaluation, we concluded that OAC-P performs as expected for all datasets. There is a clear coherence in the characterization of the pycnocline, with temporal and/or spatial continuity. Pycnocline properties are very rarely estimated where a subtropical pycnocline is not expected to exist. OAC-P performs well also in all subtropical gyres. A brief report on OAC-P implementation in all other subtropical gyres is given in appendix C.

5. The pycnocline in the North Atlantic revealed by Argo data

To describe the structure of the pycnocline in the North Atlantic subtropical gyre, we applied OAC-P to the 147 069 Argo profiles selected in the North Atlantic (see section 2; the spatial density of the collection of the 147 069 Argo profiles is shown in Fig. 6a). Then, all estimated properties were mapped onto a regular grid. Pointwise results are described in section 5a, mapped structural properties (pycnocline depth and thickness) in section 5b, and mapped thermohaline properties at the depth of the pycnocline in section 5c.

a. *Pointwise pycnocline properties*

After the QC procedure, we obtained pycnocline property estimates for 57 297 profiles. Figure 6b shows the spatial density of the collection of the 57 297 profiles. The spatial density is such that there are around 30 profiles per 1° × 1° cell over most of the North Atlantic subtropical gyre. Profiles for which no surface mode water could be characterized are mostly found out of the subtropical gyre (not shown), which underlies the good achievement of OAC-P in the detection of typical subtropical profiles. Almost no (subtropical) permanent pycnoclines are identified by OAC-P in the tropics between 10° and 20°N. There are fewer profiles with estimates of pycnocline properties in the Labrador and Irminger Seas and in the equatorial region than in the subtropics. Figures 6c and 6d show the seasonal and interannual sampling of these profiles with pycnocline property estimates, respectively. The dataset has between

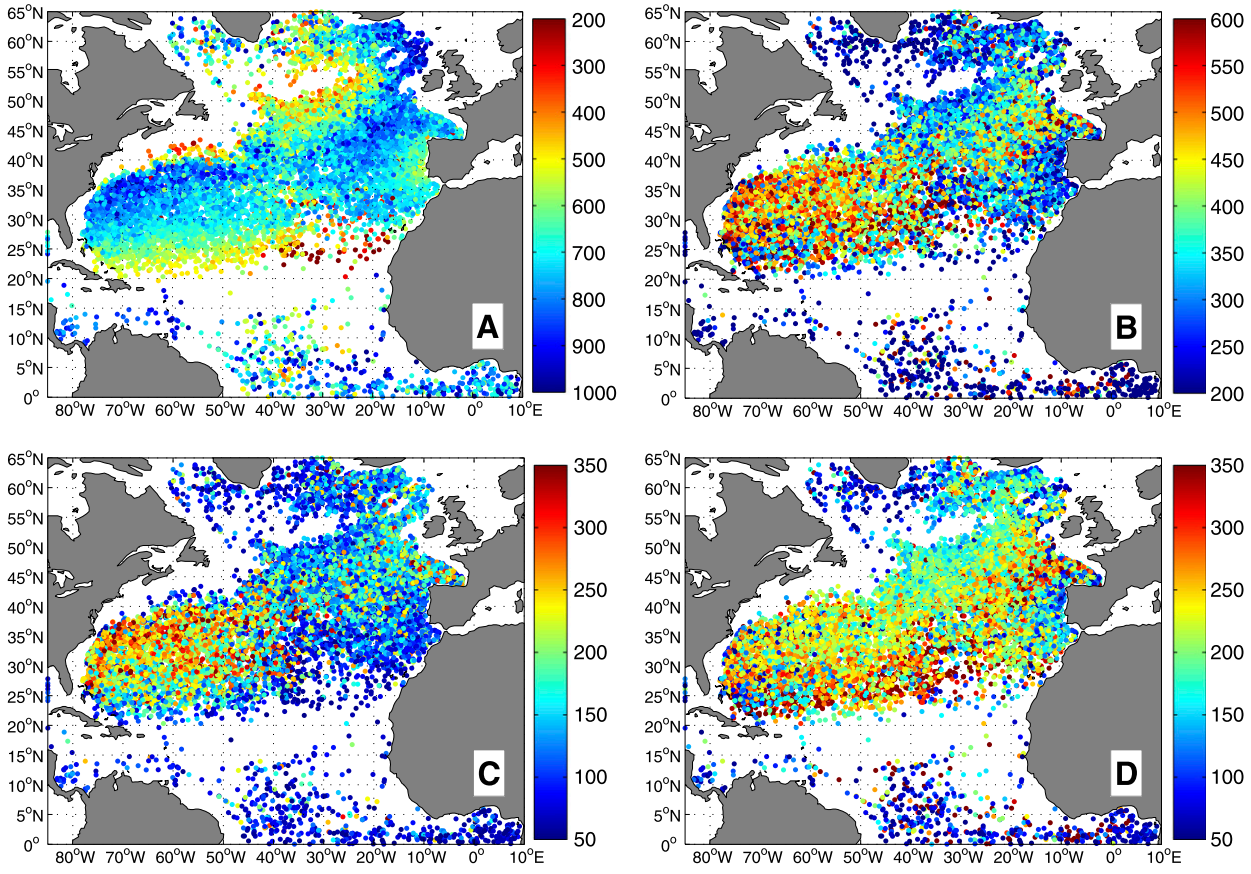

FIG. 7. Pycnocline property estimates (m): (a) depth, (b) total thickness, (c) top thickness, and (d) bottom thickness. Only one profile out of five has been plotted to reduce clutter.

4000 and 5000 profiles with pycnocline property estimates per month, without a significant seasonal bias. The continuous increase in the number of profiles with pycnocline property estimates per year reflects the Argo dataset buildup.

Figures 7 shows post maps of the depth, total thickness, and top and bottom thicknesses of the pycnocline in individual profiles. A large-scale coherent pattern emerges for each of these properties. This pattern is in line with the pycnocline structure characterized in the evaluation of OAC-P (Fig. 5) with a large-scale shoaling/thinning of the pycnocline near the Gulf Stream, the North Atlantic Current, and along the southern boundary of the gyre and deep/thick pycnoclines at the center of the gyre.

The number of profiles with pycnocline property estimates located out of the subtropical gyre amounted to around 10%, mostly in the equatorial and subpolar regions. As the focus of this study is the subtropical gyre pycnocline, we had to remove these profiles from our dataset. To do so, we used a classification method (a Gaussian mixture model) to label profiles according to their probability of belonging to a given cluster of pycnocline thermohaline properties (see appendix A for more details). Profiles within the equatorial and subpolar regions were automatically classified into a specific cluster (see Fig. A1) that was simply excluded from the rest of the analysis.

All subtropical pycnocline property estimates from the dataset were finally mapped onto a regular 0.5° × 0.5° grid using a simple Gaussian weighted mean with a standard deviation set to 0.5°. Gridpoint mapping was limited to a 0.5° radius disk containing at least six point values, leaving some grid points empty rather than filled with doubtful interpolation. We computed property error as a Gaussian weighted standard error using a decorrelation time scale of 3 months to compute the number of independent observations. This error represents both spatial and temporal variability within the 0.5° radius disk. These maps are our 2000–14 reference products of pycnocline properties that we now describe and analyze. Data can be downloaded (see Feucher et al. 2016).

b. *Structure of the pycnocline*

The 2000–14 mean depth and total thickness of the pycnocline are shown in Fig. 8, together with their

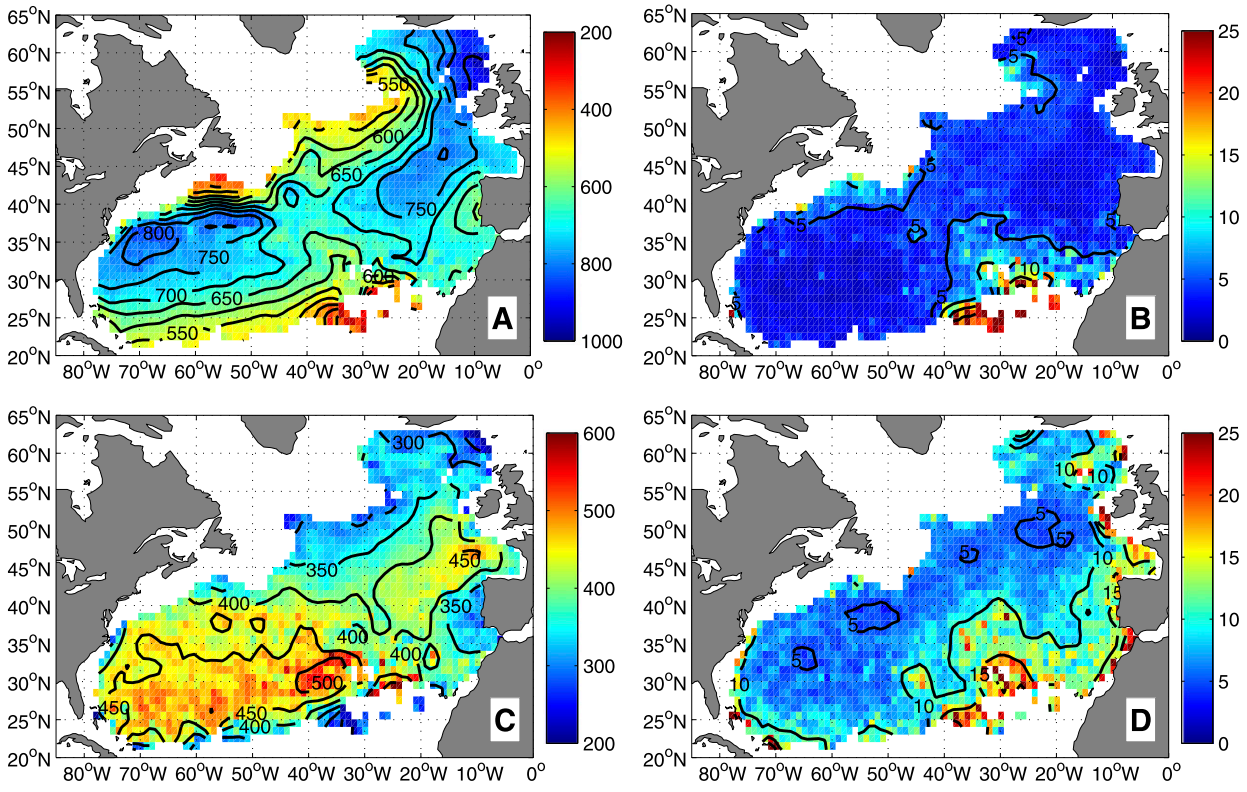

FIG. 8. Mapped pycnocline properties: (a) pycnocline depth (contours every 50 m) and (b) its relative error (%, contours every 5%), and (c) pycnocline total thickness (contours every 50 m) and (d) its relative error (%). The total thickness is the sum of the top and bottom thicknesses (shown in Fig. 9).

relative errors. We first note that the North Atlantic pycnocline extends throughout the subtropical gyre. It is limited to the north by the GSE and the North Atlantic Current, west and east of Newfoundland, respectively. On the southern flank of the gyre, the pycnocline is limited by the North Equatorial Current, which flows westward along a line going from the Canary Islands to Puerto Rico. Within this latitudinal range, the pycnocline extends zonally from coast to coast. It reaches as far as the Reykjanes and Iceland–Scotland Ridges in the extreme northeastern part of the gyre.

At the basin scale, the pycnocline is the deepest (down to 800 m) in the middle and shoals poleward and equatorward (up to 550 m). This pattern is very robust with a relative error smaller than 5% throughout the gyre, except in the southeastern corner, where it is between 5% and 10%. This mean large-scale structure is reminiscent of the classic bowl shape of a subtropical gyre pycnocline forced by a negative wind stress curl (e.g., Vallis 2006). OAC-P additionally shows that the total pycnocline thickness broadly follows a similar structure, although local extremes do not coincide. The total thickness is thicker in the center (around 450 m) and thinner along the edges (around 200 m). Again, this pattern is robust with a relative error smaller than 10% throughout the gyre, except in the southeastern corner and around Rockall Plateau, where it is between 10% and 15%.

At the regional scale, a much more complex pycnocline structure emerges. Regions with different depth/thickness distributions and relations can be identified. To explain the local patterns of the total thickness, Fig. 9 shows the 2000–14 mean top and bottom thicknesses, together with their relative errors. Figure 9e additionally shows the relative contribution of the top layer to the total thickness. We used this metric as a measure of the vertical asymmetry of the top and bottom layers around the pycnocline depth, and we refer to it as an asymmetry percentage. From these maps, we identified several key regions.

- The northeastern corner of the subtropical gyre. There, the pycnocline is the deepest, from 700 to around 900 m, especially along the eastern branch of the North Atlantic Current, in Rockall Trough. But it is relatively thin, from 300 to 350 m, mostly because the bottom thickness is small (from 150 to 200 m) compared to the rest of the gyre, while the top

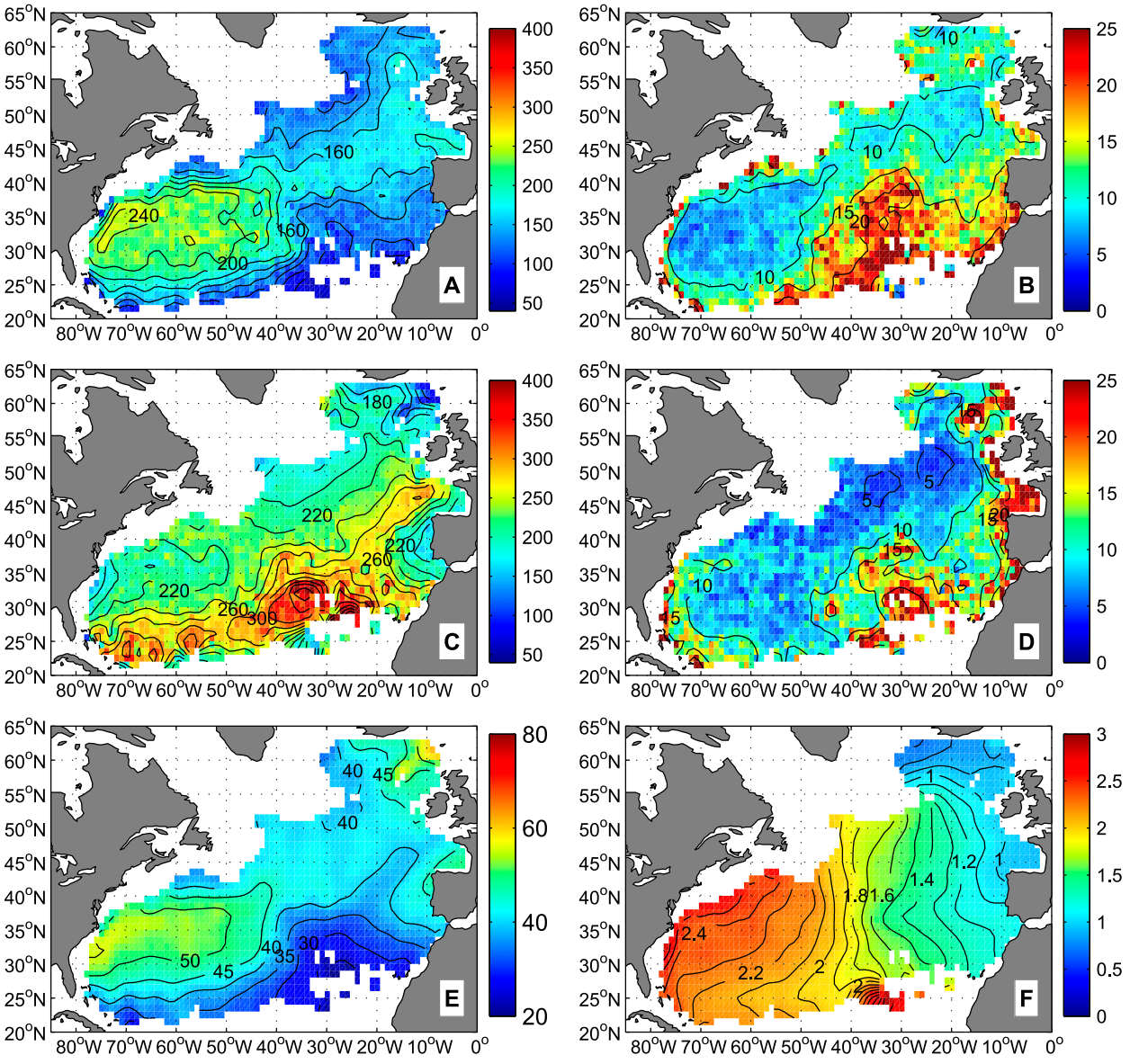

FIG. 9. (a) Pycnocline top thickness (contours every 20 m) and (b) its relative error (%, contours every 5%). (c) Pycnocline bottom thickness (contours every 20 m) and (d) its relative error (%, contours every 5%). (e) Relative contribution of the top thickness to the total thickness (%, contours every 5%). (f) Stratification amplitude at the depth of the pycnocline (N^2 in $10^{-5}\,s^{-2}$, contours every $0.1 \times 10^{-5}\,s^{-2}$).

thickness is only around 100–150 m thick. In this region, relative errors are around 5%–10% for both thicknesses, except in the Rockall Plateau area, where it is between 10% and 15%. Outside of this more uncertain area, the pycnocline is asymmetric with the upper layer representing between 40% and 50% of the total pycnocline thickness.

- The West European Basin: from 50°N, 10°W to the Azores Islands. In this region the pycnocline is deep (from 750 to 800 m) and thick (from 400 to 450 m). Both the top and bottom layers of the pycnocline are thicker than average over the gyre (around 180 and 260 m, respectively). As the bottom thickness is significantly larger than the top one, the pycnocline is strongly asymmetric (between 40% and 45%) in this region. Relative errors are around 10%.
- The southern recirculation gyre of the GSE, down to 30°N, or Bermuda, and west of 45°W. In this region, the pycnocline is deep (from 700 m at 30°N to 850 m on the equatorward flank of the GSE) with two local maxima at 67° and 55°W. The total thickness is relatively constant around 450 m. The pycnocline is symmetric around its depth in the eastern part of this region (55°–45°W), but it quickly becomes strongly

asymmetric in the western part (60°W) because the top thickness is particularly large there (around 240 m, more than 55% of the total thickness). This region is also where the relative error is the smallest for all estimates (less than 10%). This region is flanked to the north at 55°W by an area where the pycnocline rapidly shoals and thins through the GSE.

- The southwestern corner of the gyre: south of 30°N and west of 40°W. There, the pycnocline is characterized by a southward shoaling depth (from 700 up to 550 m), and a relatively constant and large total thickness of 475 m (although rapidly decreasing to 350 m along the southern edge). The stable total thickness is due to a counterbalance between a southward-decreasing top and a southward-increasing bottom thickness. Thus, the vertical asymmetry increases southward, the top thickness accounting for 50% at 30°N down to 35% at the southern edge of the region. Relative errors are around 10%, but they are slightly larger than in the previous region of the GSE recirculation gyre.
- The mid-Atlantic region extending from the Mann eddy at 41°N, 43°W [Mann (1967), where the GSE splits between the North Atlantic Current and the Azores front] down to 35°N, 35°W. This region is flanked to the west by the southern recirculation gyre of the GSE and to the east by the West European Basin, while it is limited southward by the Azores Current at 32°N (Klein and Siedler 1989). Pycnocline characteristics of the region are intermediate, with a depth and a total thickness of 675 and 400 m, respectively. The asymmetry is 45%. We can see the Mann anticyclonic eddy signature in the pycnocline depth as a 700-m local maximum.
- The equatorward flank of the North Atlantic Current, between 45° and 25°W down to 45°N. Compared to the rest of the gyre, this is a region where the pycnocline is shallow and thin. Locally, the pycnocline shoals northward from 600 up to 400 m and thins from 375 to 300 m. The pycnocline thinning is observed both in the top and bottom layers with a constant asymmetry between 40% and 45%. This region is where the relative error on the bottom thickness is the smallest, less than 5%.
- The Mediterranean outflow region (Daniault et al. 1994). There, the pycnocline is relatively shallow (around 650 m) and thin (around 330 m). This region is characterized by a bottom layer that is particularly thin, less than 200 m. On the other hand, the region has no clear signature in the top thickness, which is relatively thin in the entire southeastern corner of the gyre. This explains why the asymmetry is around 45%. Relative errors are higher than usual, especially along the Portugal coast.
- The last distinct region extends on the equatorward flank of the Azores Current at 32°N, from the Canary Islands to 40°W. In this region, the pycnocline is shallow (600 m) and thin (350 m). Relative errors are the highest in this region: more than 15% for all properties, as high as 20% for the top thickness.

For the structural description of the pycnocline to be complete, Fig. 9f shows the amplitude of N^2 at the depth of the pycnocline. At the basin scale, OAC-P reveals that the pycnocline is much more stratified in the western basin than in the eastern basin. The northeastern corner of the subtropical gyre is the region where the pycnocline has the smallest stratification amplitude ($0.9 \times 10^{-5}\,s^{-2}$), while the pycnocline has the largest stratification amplitude ($2.5 \times 10^{-5}\,s^{-2}$) in the GSE. It is worth noting that over the western basin, west of 40°W, the stratification gradient is mostly meridional, increasing from 25°N toward the GSE. Over the eastern basin, the stratification gradient is mostly zonal: increasing westward from 1 to $1.8 \times 10^{-5}\,s^{-2}$.

c. *Thermohaline properties of the pycnocline*

We now describe thermohaline properties of the pycnocline. Figure 10 shows maps of temperature (Fig. 10a), salinity (Fig. 10b) and potential density anomaly σ_0 (Fig. 10c) at the depth of the pycnocline. In the western part of the subtropical gyre, from the GSE to 25°N and west of 40°W, the temperature increases southward from 11° to 13.5°C, the salinity from 35.4 to 35.8, and the potential density anomaly decreases from 27.1 to $26.9\,kg\,m^{-3}$. The southern recirculation gyre of the GSE is homogeneous in temperature and salinity, hence in density. This region coincides with a very deep pycnocline (Fig. 8a) and an upper layer that is particularly thick (Fig. 9a). West of 40°W, most of the meridional gradient in thermohaline properties is concentrated south of 31°N. It is such that the pycnocline density decreases. Hence, one will note that the pycnocline core shoals southward along a steeper slope than isopycnal surfaces, while, on the other hand, the pycnocline shoaling across the GSE is mostly along isopycnals (there is no clear meridional density gradient at the pycnocline depth in the frontal region). As for structural properties, 40°W marks a clear transition for thermohaline properties between the western and eastern parts of the subtropical gyre. This transition also coincides with a clear change in the amplitude of the pycnocline stratification (Fig. 9f). To the east of the Mid-Atlantic Ridge, the thermohaline property gradient is oriented along a northwest/southeast axis. Although shallower than in the west, the eastern pycnocline is colder with temperatures ranging from 7°C in the Iceland basin to 11°C off the Iberian Peninsula. Salinity also increases, from 35.1 to 35.8. In the West European Basin, temperature and salinity

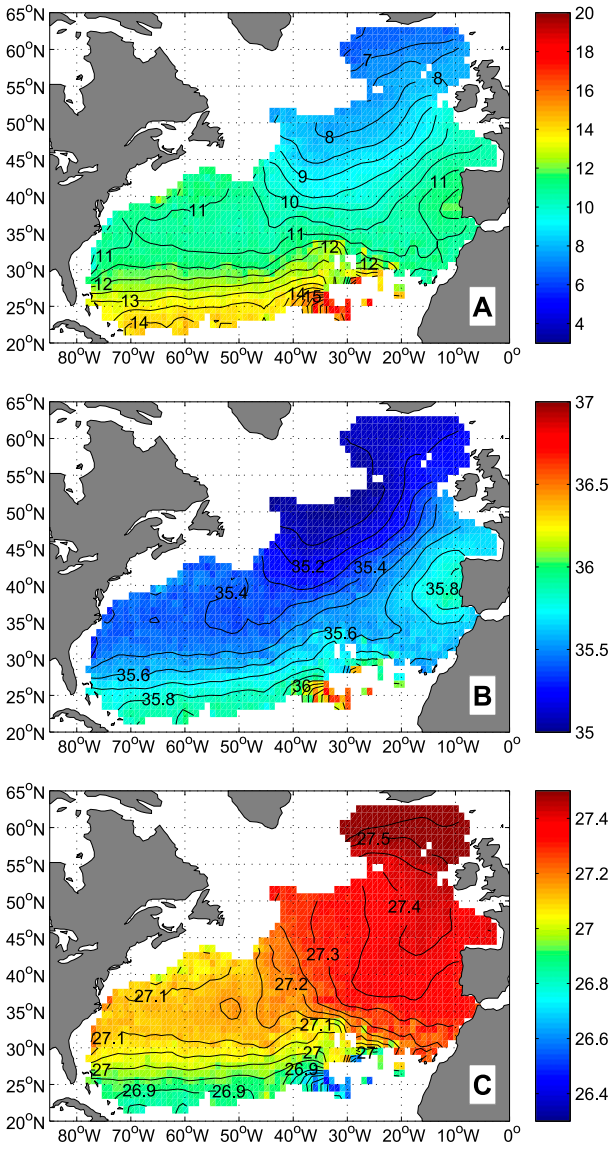

FIG. 10. Thermohaline properties at the depth of the pycnocline. (a) Temperature, contours every 0.5°C. (b) Salinity, contours every 0.1. (c) Term σ_0, contours every 0.05 kg m^{-3}.

gradients compensate each other to create a region of relatively constant pycnocline potential density anomaly around 27.4 kg m^{-3}. Similar to the southern recirculation gyre of the GSE, this region coincides with a very deep pycnocline. In the Mediterranean outflow region, a warmer (11.5°C) and saltier (35.8) pycnocline is observed. This region coincides with a shallow pycnocline (Fig. 8a) and a bottom layer that is particularly thin (Fig. 9c), probably because of the Mediterranean outflow water found just below (Potter and Lozier 2004). North of 50°N and in the Iceland Basin, the pycnocline salinity is homogenous around 35.15 and the temperature decreases northward from 8° to 6.5°C. This leads to a positive poleward density gradient at the pycnocline depth, from 27.45 up to 27.55 kg m^{-3}. In the southeastern part of the gyre, in the Azores Current region, the pycnocline temperature is homogenous around 11°C and the salinity decreases away from the Iberian Peninsula, from 35.8 down to 35.6. This leads to a negative equatorward density gradient at the pycnocline depth, from 27.4 down to 27.25 kg m^{-3}.

By definition, the pycnocline is a stratified transition layer between homogeneous water masses. Therefore, we do not expect the temperature/salinity properties at the depth of the pycnocline to correspond to a single water mass (i.e., a mode in the T/S plan). Instead, we expect pycnocline T/S properties to primarily reflect mixing between surface and deep source waters. These, in turn, are clearly identified (Fig. 11a). The deep water is the UNADW: a mixture of LSW, AAIW, and MW (Talley et al. 2011). Surface mode waters are the EDW, the eastern North Atlantic Central Water (its 12° and 16°C flavors: ENACW12 and ENACW16, respectively), and the SPMW (its 8° and 10°C flavors: SPMW8 and SPMW10, respectively; García-Ibáñez et al. 2015). A detailed description of the surface mode waters as identified by OAC-P is given in appendix B. Figure 11a shows the T/S diagram at the depth of the pycnocline. Aforementioned source waters are indicated by the overlaying black dots. The diagram uses all the data points used for the mapping, not for the mapped fields. The pycnocline T/S distribution is complex. A strongly stratified branch with intermediate salinity values extends at temperatures higher than 12°C. This part of the diagram corresponds to the southernmost region of the pycnocline, south of 28°N (Fig. 10a), where it shoals toward the North Equatorial Current. The warmest/saltiest tip of this branch is due to the particularly light/shoal pycnocline observed between 30° and 40°W. The rest of the diagram clearly lies within mixing triangles or along mixing lines of the different source waters. All identified surface waters do not operate in all regions. For instance, the SPMW8 is only a source water for the coldest part of the diagram that corresponds to the northeastern pycnocline.

It is not straightforward from this diagram to determine where the pycnocline, as defined here by a stratification maximum, follows isopycnal surfaces. To help us to do so, we can assume that if the maximum of stratification is along an isopycnal surface, it is likely that it will also have a relatively constant stratification value (that would reflect small variations of the local density structure). Figure 11b shows the σ_0/N^2 diagram at the depth of the pycnocline. We superimposed contours of the probability density function (PDF) of the dataset

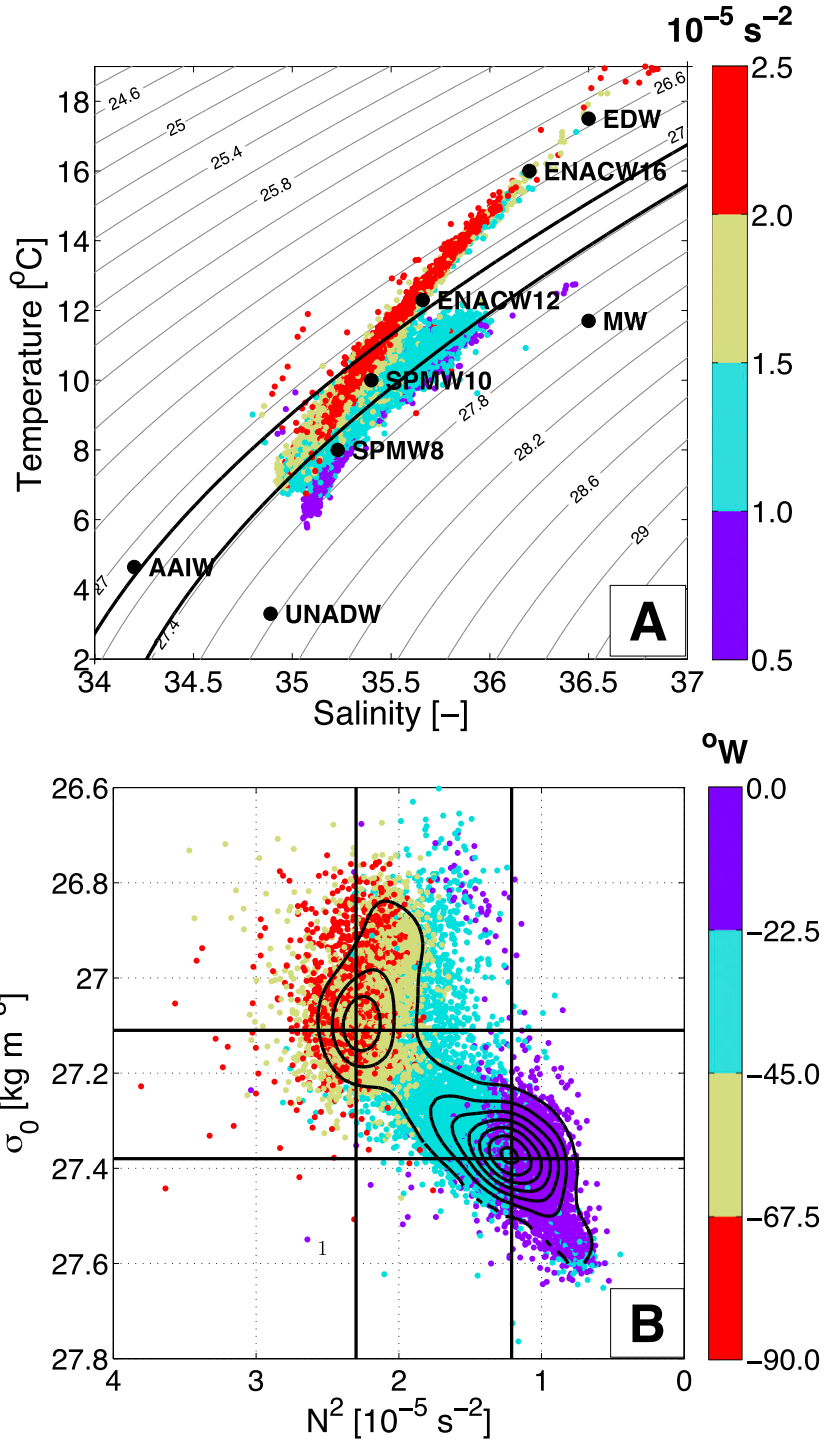

FIG. 11. (a) Temperature–salinity diagram at the depth of the pycnocline with the amplitude of the stratification N^2 as the color scale. Surface and deep source waters are indicated by black dots: EDW, ENACW16 and ENACW12, MW, SPMW10 and SPMW8, AAIW, and UNADW. Isopycnals are shown in light gray (contours every 0.2 kg m^{-3}) with the 27.11 and 27.36 kg m^{-3} isopycnals of the western and eastern pycnoclines, respectively, highlighted in black. (b) Term σ_0 vs stratification N^2 diagram at the depth of the pycnocline with longitude as color scale. Black contours are the normalized PDF in this plan. The two horizontal black lines indicate the σ_0 of the western and eastern pycnoclines, respectively. The two vertical black lines indicate the stratification N^2 of the western and eastern pycnoclines, respectively. Note the reversed x axis in order to place the highly stratified western pycnocline to the left of the plan.

within this plan (PDF data can be downloaded, see Feucher et al. 2016). The density range of the pycnocline is very wide, from 26.8 to 27.6 kg m^{-3}, as we already have seen in Fig. 10c, and the stratification varies from 0.5 to 2.5×10^{-5} s^{-2}. The diagram is also color-coded with the longitude of profiles. It can be noted that the relative density range west of 40°W is similar to that found to the east: around 0.4 kg m^{-3}. On the other hand, stratification varies over a much smaller range to the west than to the east of 40°W (20% vs 100% in relative amplitude).

The PDF contours in this bivariate plot reveal two regional clusters of N^2 (Fig. 9f) and density (Fig. 10c): an eastern region centered at $\sigma_0 = 27.36$ kg m^{-3}/$N^2 = 1.2 \times 10^{-5}$ s^{-2} and a western one centered at $\sigma_0 = 27.09$ kg m^{-3}/$N^2 = 2.2 \times 10^{-5}$ s^{-2}. These isopycnals are highlighted on the T/S diagram in Fig. 11a. The pycnocline properties on the eastern isopycnal encompass a wide range of temperature and salinity values, while they correspond to near-isothermal and near-isohaline surfaces on the western one. Using Fig. 10, we can assert that these two isopycnals encompass a significant portion of the subtropical gyre in the West European Basin region and the GSE southern recirculation gyre, respectively. Last, we note that at 35°N, the pycnocline temperature is between 10° and 11°C throughout the subtropical gyre, and hence the density difference between the eastern and western pycnoclines is mostly due to a higher salinity in the east induced by the MW (35.6 vs 35.4).

6. Discussion

a. On OAC-P

In this study we proposed an empirical definition of the subtropical pycnocline and an objective algorithm to determine its characteristics. The pycnocline depth is defined as a local stratification maximum in the water column, trapped between a surface mode water and deep water. This complex vertical structure was never addressed as such with an objective algorithm. Indeed, previous pycnocline, or thermocline, detection algorithms focused on tropical/equatorial shallow and single stratification peak (Fiedler 2010) or on smooth monotonic profiles (Fučkar 2010).

We presented the algorithm and how to implement it in the North Atlantic Ocean with Argo data. Beyond the visual inspections of the estimated results, such as those shown in Fig. 5, we can discuss quantitatively whether OAC-P detects a pycnocline when it should. The area covered by mapped pycnocline properties in Fig. 8 captures the horizontal extent of the subtropical gyre. Within the gyre thus identified, we counted 70 292 Argo profiles. A pycnocline has been characterized by OAC-P for 78% of these profiles, while only 1% of the profiles have bad or suspicious values rejected by the QC procedure. This is a significant achievement of the algorithm. OAC-P is able to estimate most of the subtropical profiles but 21% are still missed, mostly because no surface mode water is detected. It is rather difficult to determine how many profiles within these 21% actually have a surface mode water.

Most of the 21% missed profiles are localized along the edges of the subtropical gyre (not shown). Indeed, it is difficult to identify the pycnocline near the fronts or along the edges of the gyre because the surface mode water progressively vanishes and the pycnocline shoals throughout these regions. Although we doubt that all missed profiles actually have a surface mode water to be identified, there is room for further refinements to the algorithm in order to reduce that fraction of missed profiles. For instance, OAC-P uses parameters fixed in space. This implies that OAC-P cannot describe the pycnocline as efficiently in the central recirculation region as at the boundaries of the subtropical gyre. This could be improved with, on the one hand, a smaller smoothing parameter that would decrease the detection threshold of the stratification difference between the surface mode water and the pycnocline. On the other hand, if the deepest expected depth of the surface mode water were location dependent, then we could reduce the number of situations where a shallow pycnocline is missed, typically along the edges of the gyre. One should note, however, that both refinements would come at the expense of objectivity with the addition of location-dependent parameters.

Another key point of the proposed algorithm is that the pycnocline thickness is determined (i) using a nonlinear analytical Gaussian model of the stratification profile and (ii) independently for the upper and lower layers of the pycnocline. Beyond the agreement between this model and observed profiles (other tested models, such as Lorentz curves, perform less satisfactorily) lie more physically meaningful arguments. The pycnocline is a transition layer between two homogeneous reservoirs: the surface mode water and deep waters. It is reasonable to assume that diapycnal diffusion is the leading mechanism controlling the density transition profile between these reservoirs. In this scenario, any analytical function solution to the diffusion equation is a candidate to model the equilibrium density transition profile between the two homogeneous reservoirs. The complementary error function is such a function and, as its derivative, the Gaussian curve is one possible model for the stratification profile. Figure 3 shows that this model is indeed appropriate.

The standard deviation of a Gaussian curve is a statistically meaningful, and commonly used, measure of

dispersion. This provides an intuitive link between the model parameter (the standard deviation) and the length scale of the observed profile we want to characterize (the pycnocline thickness). For instance, our model implies that the total pycnocline thickness, the sum of the standard deviations for the upper and lower parts, corresponds to the layer where around 68% of the density difference between the surface mode water and deep waters is reached (the interval limited by one standard deviation on each side of the Gaussian peak corresponds to 68.27% of the cumulative probability density function, the model of N^2 profile in this case). Last, we may also point to the fact that in the limit case of a null standard deviation, the Gaussian curve tends toward a Dirac function that corresponds to the derivative of a step function for density profiles. This limit case provides a bridge between the continuous reality and a two-layer system with two homogeneous reservoirs of finite volumes representing the surface mode water and deep waters, and no diabatic processes to transform one water mass into the other.

In the same manner that OAC-P parameters could be made location dependent to improve the performance of the parameter estimation, one could imagine that a more appropriate stratification model could be used locally to improve the fit of a parametric nonlinear function to the observed N^2 profile. Indeed, although the Gaussian model is appropriate for most of the North Atlantic Ocean, it seems less suited in the frontal region of the Gulf Stream for the upper layer of the pycnocline and along the southern boundary of the gyre for the lower layer of the pycnocline (not shown). However, a location-based stratification model would make very difficult the interpretation of the results, especially regional differences. To objectively improve how OAC-P resolves boundaries of the subtropical pycnocline, using locally more appropriate parameters or stratification models, thus remains to be explored in future studies.

b. *On the North Atlantic pycnocline*

With regard to OAC-P results in the North Atlantic Ocean, the pycnocline depth estimate confirms the large-scale historical description of the pycnocline, the classic bowl shape (Sprintall and Cronin 2001). However, OAC-P provides new additional information with regard to the pycnocline thickness and to its regional-scale properties. We detailed the depth, and top and bottom thicknesses of the pycnocline for the entire subtropical gyre, and we identified eight regions with different characteristics: the Iceland Basin, the West European Basin, the southern recirculation gyre of the GSE, the southwestern corner of the gyre, the Mid-Atlantic Ridge region, the equatorward flank of the North Atlantic Current, the Mediterranean outflow region, and the Azores Current.

The pycnocline layer covers continuously a large area while clearly encompassing a large range of properties. This suggests that, although the pycnocline is created by large-scale processes, such as the negative wind stress curl (e.g., Luyten et al. 1983) and the thermohaline circulation (e.g., Salmon 1990), local processes significantly influence and modify the textbook description of the pycnocline. For instance, Samelson and Vallis (1997) found in their analytical model that dynamic and thermodynamic processes controlling the formation of the surface mode water are indeed different between the GSE and along the eastern region of the subtropical gyre. The present results highlight that this may also affect the pycnocline.

Therefore, it is not surprising that one of the key results of the pycnocline property estimates is that the pycnocline is not centered around the depth of maximum stratification but has a vertically asymmetric structure. The asymmetry increases from 35% to 55% (smaller than 50% means that the lower layer is thicker than the upper one) and is the most pronounced in the eastern part of the subtropical gyre and along its southern boundary. The observed asymmetry supports the idea that different processes act upon the upper and lower layers of the pycnocline. For instance, similar background diffusions can be altered by different reservoir ventilation mechanisms to produce different stratifications. This may happen when the mechanical wind forcing is not in phase with surface diabatic buoyancy fluxes (Cessi 2007) or because across-gyre transports are much larger in the east than in the west, hence modifying how surface mode waters are created and how deeper layers are ventilated there (Samelson and Vallis 1997). On the other hand, the southern recirculation region of the GSE is remarkably symmetric, possibly highlighting the role of potential vorticity homogenization and eddy-induced diapycnal fluxes in thickening the pycnocline top thickness in this region, where the Gulf Stream baroclinic instability is very strong (Pedlosky and Young 1983; Radko and Marshall 2004).

We also noted that in the southwestern corner of the gyre, meridional gradients in thermohaline properties are such that the pycnocline density decreases southward. This means that the pycnocline core shoals southward along a steeper slope than isopycnal surfaces and suggests that the meridional stratification structure may be subject to other dynamical constraints than a conserved potential vorticity driving the slope of isopycnal surfaces.

Last, one can note that the relative importance of temperature and salinity in determining the stratification of the pycnocline was not assessed. Thermohaline properties at the depth of the pycnocline indicate a clear role of the salinity in the eastern part of the gyre. This is not surprising, and it highlights the crucial role played by the

Mediterranean overflow water in determining stratification in the North Atlantic Ocean.

7. Conclusions

One of the results of the pycnocline property estimates conducted in this study is that the North Atlantic pycnocline cannot be approximated by a single isopycnal surface. This demonstrates the OAC-P utility by ruling out any attempt to describe subtropical pycnocline changes using a representative isopycnal method at the basin scale. Although there is room for further improvements, we believe OAC-P will be useful for determining accurately seasonal, interannual and longer-term changes of the pycnocline in observations and numerical simulations.

In particular, OAC-P will help to describe stratification changes over decadal time scales in climate projections by providing a much more detailed analysis than the simple description of density difference between the surface and one deep depth level (e.g., Matear and Hirst 2003; Capotondi et al. 2012). By accurately describing the pycnocline as a stratified feature, it will be possible to disentangle the contradictory changes described using isopycnal vertical migration alone (e.g., Yang and Wang 2009). Last, we hope that the N^2/σ_0 diagram presented in this study will provide a synthetic view of the observed North Atlantic pycnocline to be used as a benchmark for the validation/evaluation of realistic model simulations.

Acknowledgments. We thank Paul C. Fiedler for kindly sharing his data during the development and evaluation phase of OAC-P. We also thank R. Schopp and C. Maes for their valuable discussions and feedbacks. Thanks are given to the BATS team and to the WOCE program for making BATS/Hydrostation S time series and WOCE sections freely available online. Argo data were collected and made freely available by the International Argo Program and the national programs that contribute to it (http://www.argo.ucsd.edu, http://argo.jcommops.org). The Argo program is part of the Global Ocean Observing System. C. Feucher and G. Maze were supported by L'Institut Français de Recherche pour l'Exploitation de la Mer (Ifremer), and H. Mercier was supported by the French Centre National de la Recherche Scientifique (CNRS).

APPENDIX A

Pointwise Dataset Filtering with a Gaussian Mixture Model

As shown in Fig. 5, OAC-P performed on the Argo dataset mainly provides validated results in the subtropical gyre, as expected, but also in the tropics and subpolar regions. This is due to profiles with a qualitative structure corresponding to typical profiles of the subtropical gyre, although clearly not within that gyre. These spurious estimates must be removed from the collection of profiles to be analyzed and possibly mapped to characterize the subtropical pycnocline. Using a criteria based on the position of spurious profiles in order to removed them would be clearly fastidious and in contradiction with our goal of an objective procedure. We propose using an elegant method that is based on a modal description of the results in a multidimensional plan. Indeed, pycnocline properties tend to agglomerate within clusters in the σ_0, T, S space. We can thus use an unsupervised classification method in order to identify clusters associated with spurious profiles and to remove them. To do so, we used a Gaussian mixture model (GMM) to decompose the three-dimensional probability density function of OAC-P results into a weighted sum of multivariate normal distributions (Bilmes 1998; Reynolds 2009). GMM is a widely used classification method in data mining that is gaining more and more attention in the geophysical community (e.g., Hauser et al. 2015). The GMM is trained with the following three variables:

$$\rho_{\mathrm{GMM}} = \frac{\sigma_0 + 1000}{\rho_0} - 1, \tag{A1}$$

$$T_{\mathrm{GMM}} = -\alpha(T - T_0), \tag{A2}$$

$$S_{\mathrm{GMM}} = \beta(S - S_0), \tag{A3}$$

where σ_0, T, and S are the potential density anomaly referenced to the surface, temperature, and salinity, respectively, at the depth of the pycnocline. We used $\rho_0 = 1027.3\,\mathrm{kg\,m^{-3}}$, $T_0 = 9.7°\mathrm{C}$, and $S_0 = 35.4$ (average values of the dataset). This scaling is necessary in order to work with three dimensions along which the data have comparable amplitudes. We did not use pycnocline depth and thicknesses because they do not exhibit an additional modal description of the dataset. Once trained using an optimization algorithm, GMM provides the probability for each profile to belong to N cluster; that is, we have N values (summing to one) for each profile. Figure A1 shows the maximum probability value for each profile using $N = 5$ clusters. We split the profiles according to the cluster index of that maximum probability, producing $N = 5$ maps. The choice of $N = 5$ was done by trial and error to optimize the identification of spurious profiles in separate clusters. With $N = 5$, we clearly see in Fig. A1 that clusters A, B, C, and E contain profiles within the subtropical gyre, while cluster D agglomerates all spurious profiles. We thus removed the

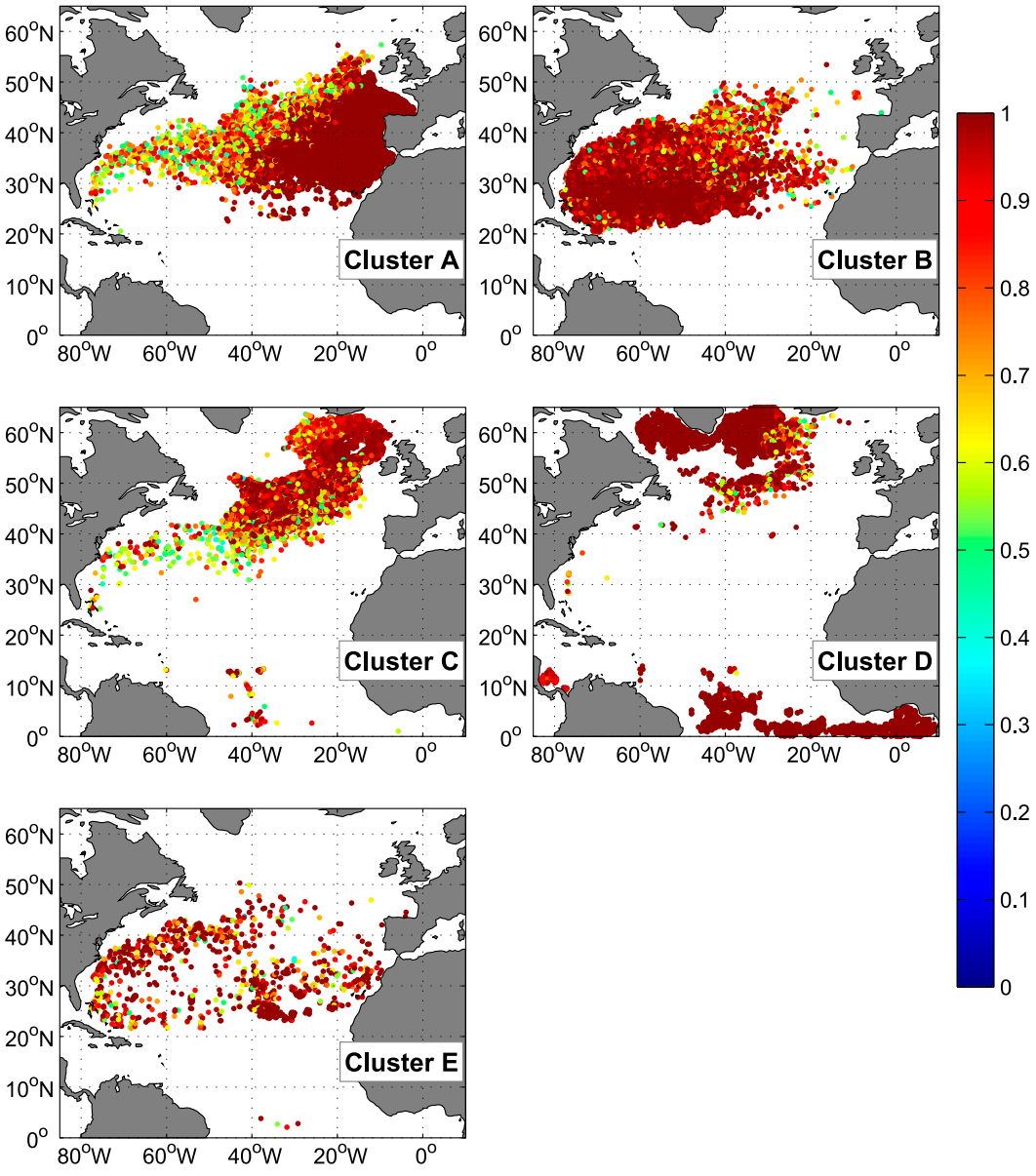

FIG. A1. Results of the GMM unsupervised classification of Argo profiles using pycnocline thermohaline characteristics. Color scale represents the posterior probability of a profile belonging to clusters A–E. This probability is defined for all profiles of the pycnocline dataset and all clusters, but for readability we plotted it only for the profiles attributed to each cluster.

profiles identified in cluster D from the dataset described in the rest of the study.

APPENDIX B

Surface Mode Waters

Given that OAC-P has to identify a stratification minimum associated with a surface mode water to estimate pycnocline properties, it is tempting to a posteriori check which water masses overlie the pycnocline. This analysis helped us to explain the thermohaline properties of the pycnocline in section 5c. Figure B1 shows the depth, density, temperature, and salinity of the surface mode waters identified by OAC-P. In the North Atlantic subtropical gyre, two surface mode waters are identified by OAC-P, all in line with the bibliographic standards as described below.

The surface mode water covering the largest area is the EDW with a depth between 300 and 350 m, and a

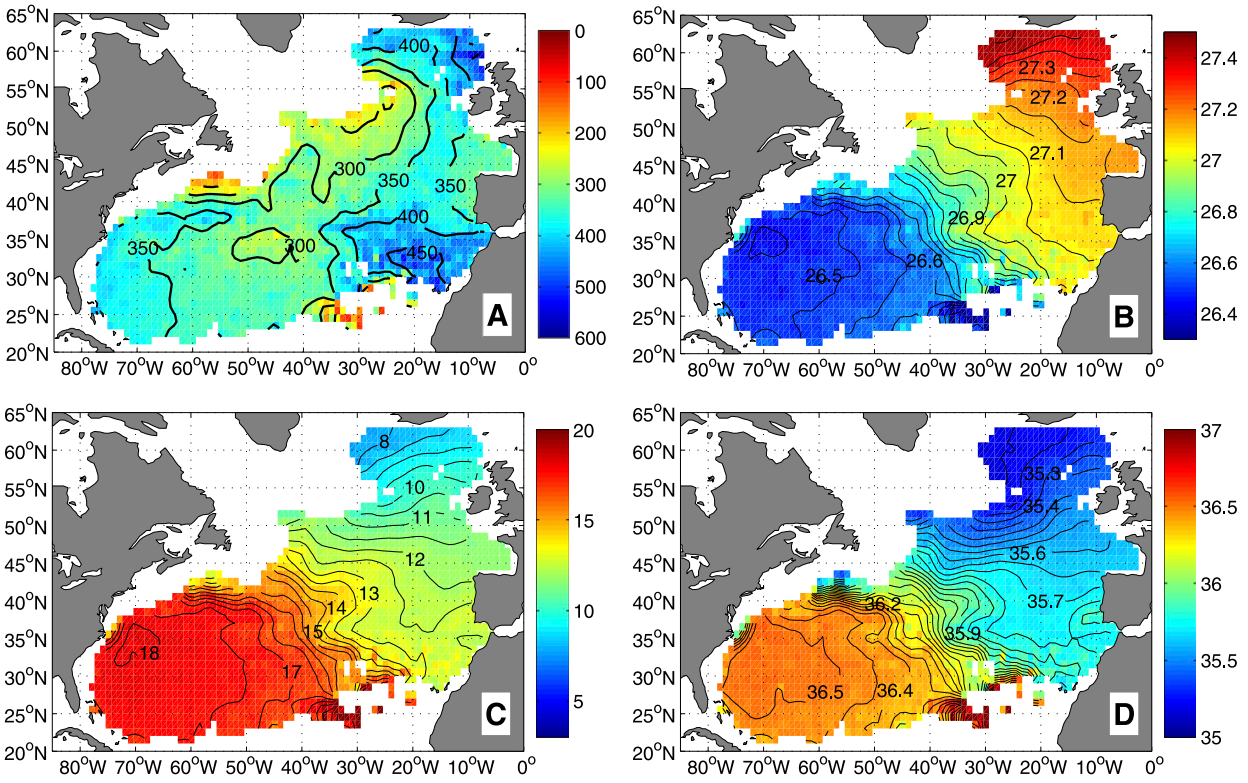

FIG. B1. Properties of the surface mode waters identified by OAC-P as overlying the pycnocline. (a) Depth with contours every 50 m. (b) Term σ_0 with contours every 0.05 kg m^{-3}. (c) Temperature with contours every 0.5°C. (d) Salinity with contours every 0.05.

density around 26.5 kg m^{-3}, a temperature of 17.5°C, and a salinity of 36.5 (Maze and Marshall 2011). The EDW is found nearly everywhere west of 40°W. We observe a shoaling of the surface mode water depth across the GSE and the North Atlantic Current that is concomitant with the shoaling and thinning of the pycnocline there. In the northeastern corner of the subtropical gyre, north of 50°N and up to the Irminger Current, OAC-P identified different flavors of SPMW as the surface mode water overlying the pycnocline (Brambilla and Talley 2008). Centered between 300- and 450-m depth, SPMWs have a core density between 27.25 and 27.45 kg m^{-3}, a temperature between 8° and 10°C, and a salinity between 35.2 and 35.4.

Along 40°W, *T*/*S* properties experience a strong zonal gradient centered on the properties of the warmest ENACW (16°C, 36.2, ENACW16). This gradient underlies a clear change in the type of surface mode water tracked by OAC-P between the eastern and western parts of the gyre. East of 40°W and south of 50°N, in the West European Basin, OAC-P captures a wide variety of central waters with the *T*/*S* relationship closely related to their formation by winter mixing in the surface layer along a wide range of latitudes (Iselin 1939). But an intermediate flavor of ENACW stands out around 350-m depth. This is the ENACW12 that has a relatively homogeneous density around 27.1 kg m^{-3}, a temperature between 11° and 13°C, and a salinity between 35.4 and 35.8. This ENACW12 corresponds to the 11°–12°C lower central mode water subducted in the northern part of the region and identified by Paillet and Arhan (1996) at the base of what they called a shallow *secondary* pycnocline at about 200-m depth (see their Fig. 3, for instance). In the southeastern part of the subtropical gyre, the surface mode water is the deepest, near 450 m. The Madeira Mode Water (Siedler et al. 1987) is too thin and too shallow to be captured by OAC-P.

APPENDIX C

Application of OAC-P in other Subtropical Gyres and Comparison with an Alternative Method

OAC-P has been developed to estimate pycnocline properties in subtropical gyres. Following the implementation method described in section 4, we determined an appropriate set of OAC-P parameters for each gyre. In the following, we briefly show how OAC-P can perform in each of the five subtropical gyres.

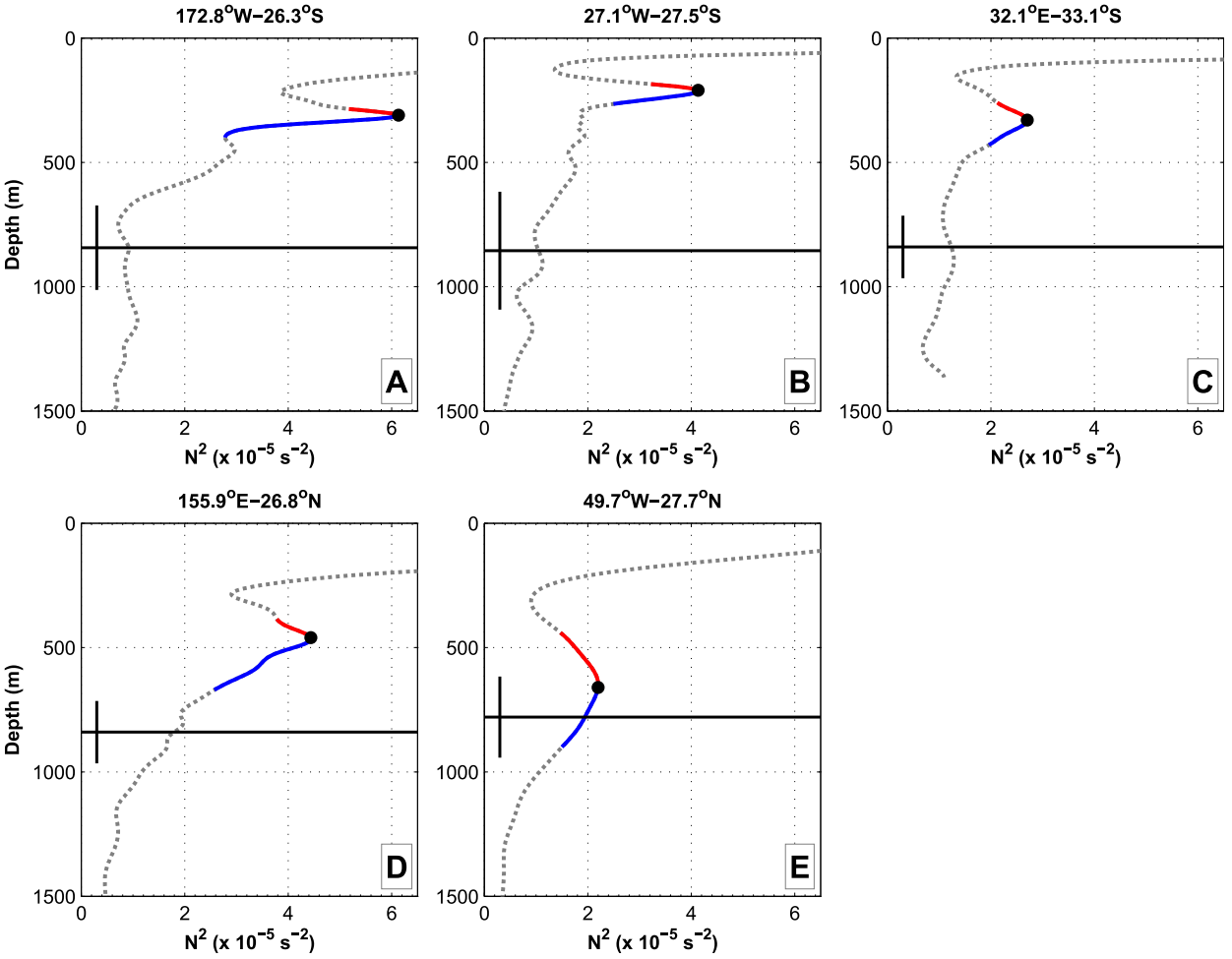

FIG. C1 . Application of OAC-P with Argo profiles in the (a) South Pacific subtropical gyre (WMO 5903574, cycle 61), (b) South Atlantic subtropical gyre (WMO 3900771, cycle 113), (c) Indian subtropical gyre (WMO 1901429, cycle 2), (d) North Pacific subtropical gyre (WMO 2902453, cycle 13), and (e) North Atlantic subtropical gyre (WMO 4900788, cycle 68). Dashed gray curves represent N^2 profiles. Black dot represents the depth of the pycnocline, and the red (blue) curve represents the upper (lower) layer of the pycnocline, as computed using OAC-P. Horizontal and vertical black lines indicate the depth and thickness scale of the pycnocline computed using Gnanadesikan (1999) and Gnanadesikan et al. (2007) methods.

Based on the description by Hanawa and Talley (2001), the main surface mode waters found in subtropical gyres are the North Atlantic Subtropical Mode Water, the South Atlantic Subtropical Mode Water, the North Pacific Subtropical Mode Water, the South Pacific Subtropical Mode Water, and the Indian Subtropical Mode Water. In the Southern Hemisphere oceans, the mode water is found to be shallower than in the Northern Hemisphere oceans. In the South Atlantic, the South Pacific, and the Indian Oceans, we found $z_{\text{inter}} = 200$ m to be the most appropriate value, while in the North Pacific Ocean, we set $z_{\text{inter}} = 400$ m. We recall that in the North Atlantic Ocean, we used $z_{\text{inter}} = 600$ m. Mode waters in the Southern Hemisphere oceans are also thinner than in the Northern Hemisphere oceans. Therefore, we reduced the smoothing scale to 20 m to characterize the depth of the mode water in the South Pacific, the South Atlantic, and the Indian Oceans. In the North Pacific and North Atlantic Oceans, the smoothing scale is 50 m.

Figure C1 illustrates pycnocline property estimates (depth and thickness) in all subtropical gyres using Argo profiles in the North Atlantic (WMO 4900788, cycle 68), South Atlantic (WMO 3900771, cycle 113), North Pacific (WMO 2902453, cycle 13), South Pacific (WMO 5903574, cycle 61), and Indian Oceans (WMO 1901429, cycle 2). It is clear that OAC-P is able to characterize the pycnocline properties in all subtropical gyres. It would be interesting to compare these properties from one gyre to another but this is beyond the scope of this study.

Last, we superimposed on each profile in Fig. C1 the pycnocline depth and thickness estimates using the Gnanadesikan (1999) formulation for the depth and the Gnanadesikan et al. (2007) formulation for the thickness, as described in Fučkar (2010). Except for the North Atlantic profile, the alternative method is clearly inappropriate when applied to Argo data. This is because the Gnanadesikan (1999) and Gnanadesikan et al. (2007) methods target smooth and unimodal N^2 profiles.

REFERENCES

Argo, 2014: Argo floats data and metadata from Global Data Assembly Centre (Argo GDAC)—Snapshot of Argo GDAC of December, 8th 2014. SEANOE, accessed 11 December 2014, doi:10.17882/42182.

Balmaseda, M. A., K. Mogensen, and A. T. Weaver, 2013: Evaluation of the ECMWF ocean reanalysis system ORAS4. *Quart. J. Roy. Meteor. Soc.*, **139**, 1132–1161, doi:10.1002/qj.2063.

Bilmes, J. A., 1998: A gentle tutorial of the EM algorithm and its application to parameter estimation for Gaussian mixture and hidden Markov models. International Computer Science Institute Tech. Rep. TR-97-021, 126 pp.

Brambilla, E., and L. D. Talley, 2008: Subpolar Mode Water in the northeastern Atlantic: 1. Averaged properties and mean circulation. *J. Geophys. Res.*, **113**, C04025, doi:10.1029/2006JC004062.

Capotondi, A., M. A. Alexander, N. A. Bond, E. N. Curchitser, and J. D. Scott, 2012: Enhanced upper ocean stratification with climate change in the CMIP3 models. *J. Geophys. Res.*, **117**, C04031, doi:10.1029/2011JC007409.

Carval, T., and Coauthors, 2012: Argo user's manual. Version 2.4, Argo Reference ar-um-02-01, Ifremer Reference cor-do/dtimut/02-084, 85 pp.

Cessi, P., 2007: Regimes of thermocline scaling: The interaction of wind stress and surface buoyancy. *J. Phys. Oceanogr.*, **37**, 2009–2021, doi:10.1175/JPO3103.1.

Daniault, N., J. Mazé, and M. Arhan, 1994: Circulation and mixing of Mediterranean water west of the Iberian Peninsula. *Deep-Sea Res. I*, **41**, 1685–1714, doi:10.1016/0967-0637(94)90068-X.

De Boyer Montégut, C., G. Madec, A. S. Fischer, A. Lazar, and D. Iudicone, 2004: Mixed layer depth over the global ocean: An examination of profile data and a profile-based climatology. *J. Geophys. Res.*, **109**, C12003, doi:10.1029/2004JC002378.

Donguy, J. R., 1987: Recent advances in the knowledge of the climatic variations in the tropical Pacific Ocean. *Prog. Oceanogr.*, **19**, 49–85, doi:10.1016/0079-6611(87)90003-6.

Feucher, C., G. Maze, and H. Mercier, 2016: 2000–2014 climatology of the North Atlantic permanent pycnocline properties. SEANOE, accessed 3 June 2016, doi:10.17882/42386.

Fiedler, P. C., 2010: Comparison of objective descriptions of the thermocline. *Limnol. Oceanogr. Methods*, **8**, 313–325, doi:10.4319/lom.2010.8.313.

——, R. Mendelssohn, D. M. Palacios, and S. J. Bograd, 2013: Pycnocline variations in the eastern tropical and North Pacific, 1958–2008. *J. Climate*, **26**, 583–599, doi:10.1175/JCLI-D-11-00728.1.

Fofonoff, N. P., and R. C. Millard Jr., 1983: Algorithms for computation of fundamental properties of seawater. UNESCO Technical Papers in Marine Science 44, 54 pp.

Forget, G., G. Maze, M. Buckley, and J. Marshall, 2011: Estimated seasonal cycle of North Atlantic Eighteen Degree Water volume. *J. Phys. Oceanogr.*, **41**, 269–286, doi:10.1175/2010JPO4257.1.

Fučkar, N.-S., 2010: Adaptive scaling model of the main pycnocline and the associated overturning circulation. Ph.D. thesis, Princeton University, 251 pp.

García-Ibáñez, M. I., P. C. Pardo, L. I. Carracedo, H. Mercier, P. Lherminier, A. F. Ríos, and F. F. Pérez, 2015: Structure, transports and transformations of the water masses in the Atlantic Subpolar Gyre. *Prog. Oceanogr.*, **135**, 18–36, doi:10.1016/j.pocean.2015.03.009.

Gnanadesikan, A., 1999: A simple predictive model for the structure of the oceanic pycnocline. *Science*, **283**, 2077–2079, doi:10.1126/science.283.5410.2077.

——, A. M. de Boer, and B. K. Mignone, 2007: A simple theory of the pycnocline and overturning revisited. *Ocean Circulation: Mechanisms and Impacts—Past and Future Changes of Meridional Overturning*, *Geophys. Monogr.*, Vol. 173, Amer. Geophys. Union, 19–32, doi:10.1029/173GM04.

Hanawa, K., and L. D. Talley, 2001: Mode waters. *Ocean Circulation and Climate: Observing and Modelling the Global Ocean*, G. Siedler, J. Church, and W. J. Gould, Eds., International Geophysics Series, Vol. 77, Academic Press, 373–386.

Hauser, T., E. Demirov, J. Zhu, and I. Yashayaev, 2015: North Atlantic atmospheric and ocean inter-annual variability over the past fifty years—Dominant patterns and decadal shifts. *Prog. Oceanogr.*, **132**, 197–219, doi:10.1016/j.pocean.2014.10.008.

IPCC, 2013: *Climate Change 2013: The Physical Science Basis.* Cambridge University Press, 1535 pp., doi:10.1017/CBO9781107415324.

Iselin, C., 1939: The influence of vertical and lateral turbulence on the characteristics of the waters at mid-depths. *Eos, Trans. Amer. Geophys. Union*, **20**, 414–417, doi:10.1029/TR020i003p00414.

Jackett, D. R., and T. J. Mcdougall, 1995: Minimal adjustment of hydrographic profiles to achieve static stability. *J. Atmos. Oceanic Technol.*, **12**, 381–389, doi:10.1175/1520-0426(1995)012<0381:MAOHPT>2.0.CO;2.

Kessler, W. S., 1990: Observations of long Rossby waves in the northern tropical Pacific. *J. Geophys. Res.*, **95**, 5183–5217, doi:10.1029/JC095iC04p05183.

——, M. J. McPhaden, and K. M. Weickmann, 1995: Forcing of intraseasonal Kelvin waves in the equatorial Pacific. *J. Geophys. Res.*, **100**, 10 613–10 631, doi:10.1029/95JC00382.

Klein, B., and G. Siedler, 1989: On the origin of the Azores Current. *J. Geophys. Res.*, **94**, 6159–6168, doi:10.1029/JC094iC05p06159.

Levitus, S., and Coauthors, 2012: World ocean heat content and thermosteric sea level change (0–2000 m), 1955–2010. *Geophys. Res. Lett.*, **39**, L10603, doi:10.1029/2012GL051106.

Li, Y., and F. Wang, 2013: Thermohaline intrusions in the thermocline of the western tropical Pacific Ocean. *Acta Oceanol. Sin.*, **32**, 47–56, doi:10.1007/s13131-013-0331-3.

Luyten, J. R., J. Pedlovsky, and H. Stommel, 1983: The ventilated thermocline. *J. Phys. Oceanogr.*, **13**, 292–309, doi:10.1175/1520-0485(1983)013<0292:TVT>2.0.CO;2.

Mann, C. R., 1967: The termination of the Gulf Stream and the beginning of the North Atlantic Current. *Deep-Sea Res. Oceanogr. Abstr.*, **14**, 337–359, doi:10.1016/0011-7471(67)90077-0.

Matear, R. J., and A. C. Hirst, 2003: Long-term changes in dissolved oxygen concentrations in the ocean caused by protracted global warming. *Global Biogeochem. Cycles*, **17**, 1125, doi:10.1029/2002GB001997.

Maze, G., and J. Marshall, 2011: Diagnosing the observed seasonal cycle of Atlantic subtropical mode water using potential

vorticity and its attendant theorems. *J. Phys. Oceanogr.*, **41**, 1986–1999, doi:10.1175/2011JPO4576.1.

McPhaden, M. J., 1985: Fine-structure variability observed in CTD measurements from the central equatorial Pacific. *J. Geophys. Res.*, **90**, 11 726–11 740, doi:10.1029/JC090iC06p11726.

Mercier, H., and Coauthors, 2015: Variability of the meridional overturning circulation at the Greenland–Portugal OVIDE section from 1993 to 2010. *Prog. Oceanogr.*, **132**, 250–261, doi:10.1016/j.pocean.2013.11.001.

Paillet, J., and M. Arhan, 1996: Shallow pycnoclines and mode water subduction in the eastern North Atlantic. *J. Phys. Oceanogr.*, **26**, 96–114, doi:10.1175/1520-0485(1996)026<0096:SPAMWS>2.0.CO;2.

Pedlosky, J., and W. Young, 1983: Ventilation, potential-vorticity homogenization and the structure of the ocean circulation. *J. Phys. Oceanogr.*, **13**, 2020–2037, doi:10.1175/1520-0485(1983)013<2020:VPVHAT>2.0.CO;2.

Pérez, F. F., H. Mercier, M. Vázquez-Rodríguez, P. Lherminier, A. Velo, P. C. Pardo, G. Rosón, and A. F. Ríos, 2013: Atlantic Ocean CO_2 uptake reduced by weakening of the meridional overturning circulation. *Nat. Geosci.*, **6**, 146–152, doi:10.1038/ngeo1680.

Potter, R. A., and M. S. Lozier, 2004: On the warming and salinification of the Mediterranean outflow waters in the North Atlantic. *Geophys. Res. Lett.*, **31**, L01202, doi:10.1029/2003GL018161.

Radko, T., and J. Marshall, 2004: Eddy-induced diapycnal fluxes and their role in the maintenance of the thermocline. *J. Phys. Oceanogr.*, **34**, 372–383, doi:10.1175/1520-0485(2004)034<0372:EDFATR>2.0.CO;2.

Reynolds, D., 2009: Gaussian mixture models. *Encyclopedia of Biometrics*, S. Z. Li and A. Jain, Eds., Springer, 659–663, doi:10.1007/978-0-387-73003-5_196.

Riser, S. C., and Coauthors, 2016: Fifteen years of ocean observations with the global Argo array. *Nat. Climate Change*, **6**, 145–153, doi:10.1038/nclimate2872.

Salmon, R., 1990: The thermocline as an internal boundary layer. *J. Mar. Res.*, **48**, 437–469, doi:10.1357/002224090784984650.

Samelson, R. M., and G. K. Vallis, 1997: Large-scale circulation with small diapycnal diffusion: The two-thermocline limit. *J. Mar. Res.*, **55**, 223–275, doi:10.1357/0022240973224382.

Sarachik, E. S., and M. A. Cane, 2010: *The El Niño–Southern Oscillation Phenomenon*. Cambridge University Press, 384 pp.

Schlitzer, R., 2000: Electronic atlas of WOCE hydrographic and tracer data now available. *Eos, Trans. Amer. Geophys. Union*, **81**, 45–45, doi:10.1029/00EO00028.

Siedler, G., A. Kuhl, and W. Zenk, 1987: The Madeira Mode Water. *J. Phys. Oceanogr.*, **17**, 1561–1570, doi:10.1175/1520-0485(1987)017<1561:TMMW>2.0.CO;2.

Sprintall, J., and M. Cronin, 2001: Upper ocean vertical structure. *Encyclopedia of Ocean Sciences*, Academic Press, 3120–3128, doi:10.1006/rwos.2001.0149.

Talley, L. D., 1996: North Atlantic circulation and variability, reviewed for the CNLS conference. *Physica D*, **98**, 625–646, doi:10.1016/0167-2789(96)00123-6.

——, G. L. Pickard, W. J. Emery, and J. H. Swift, 2011: Atlantic Ocean. *Descriptive Physical Oceanography: An Introduction*, 6th ed. Academic Press, 245–301, doi:10.1016/B978-0-7506-4552-2.10009-5.

Vallis, G. K., 2006: *Atmospheric and Oceanic Fluid Dynamics: Fundamentals and Large-Scale Circulation*. Cambridge University Press, 769 pp.

Wang, B., R. Wu, and R. Lukas, 2000: Annual adjustment of the thermocline in the tropical Pacific Ocean. *J. Climate*, **13**, 596–616, doi:10.1175/1520-0442(2000)013<0596:AAOTTI>2.0.CO;2.

Weaver, A., and P. Courtier, 2001: Correlation modelling on the sphere using a generalized diffusion equation. *Quart. J. Roy. Meteor. Soc.*, **127**, 1815–1846, doi:10.1002/qj.49712757518.

Worthington, L. V., 1959: The 18° water in the Sargasso Sea. *Deep-Sea Res.*, **5**, 297–305, doi:10.1016/0146-6313(58)90026-1.

Yang, H., and F. Wang, 2009: Revisiting the thermocline depth in the equatorial Pacific. *J. Climate*, **22**, 3856–3863, doi:10.1175/2009JCLI2836.1.